Brucella EipB is periplasmic β-spiral protein required for envelope stress resistance and infection

Julien Herrou[a,#,¶], Jonathan W. Willett[a,#], Aretha Fiebig[a], Daniel M. Czyż[b], Jason X. Cheng[c], Eveline Ultee[d], Ariane Briegel[d], Lance Bigelow[e], Gyorgy Babnigg[e], Youngchang Kim[e], and Sean Crosson[a*]

[a]Department of Biochemistry and Molecular Biology, University of Chicago, Chicago, Illinois, USA.

[b]Department of Microbiology and Cell Science, University of Florida, Gainesville, Florida, USA

[c]Department of Pathology, The University of Chicago, Chicago, Illinois, USA

[d]Department of Biology, Universiteit Leiden, Leiden, Netherlands

[e]Biosciences Division, Argonne National Laboratory, Argonne, Illinois, USA

* To whom correspondence should be addressed: Sean Crosson, scrosson@uchicago.edu.

[#] Contributed equally to this work

¶ Current location: Laboratoire de Chimie Bactérienne, Institut de Microbiologie de la Méditerranée, CNRS, Marseille, France.

Running Title: *Functional characterization of DUF1849*

Keywords: TPR, DUF1849, *Alphaproteobacteria*, *Brucella*, cell envelope, stress response, PF08904

Summary (250 words)

The Gram-negative cell envelope is a remarkably diverse structure with core components that include an inner membrane, an outer membrane, and a peptidoglycan layer in the periplasmic space between. We show that a conserved DUF1849-family protein, EipB, is secreted to the periplasmic space of *Brucella*, a monophyletic group of intracellular pathogens. In the periplasm, EipB folds into an unusual fourteen-stranded β-spiral structure that contains a conserved disulfide bond. EipB has structural features that resemble the LolA and LolB lipoprotein delivery system, though the overall topology and fold of EipB is distinct from LolA/LolB. Deletion of *eipB* results in defects in *Brucella* cell envelope integrity *in vitro* and in maintenance of spleen colonization in a mouse model of *B. abortus* infection. Transposon disruption of *ttpA*, which encodes a periplasmic tetratricopeptide repeat (TPR) protein, is synthetically lethal with *eipB* deletion in *B. abortus*. *ttpA* is a known virulence determinant in *B. melitensis*, and our studies of *ttpA* deletion and overexpression strains provide evidence that *ttpA*, like *eipB*, contributes to cell envelope function in *Brucella*. We conclude that *eipB* and *ttpA* function in the *Brucella* periplasmic space to maintain cell envelope integrity and to facilitate survival in a mammalian host.

Importance (120 words)

Brucella species cause brucellosis, a global zoonosis. A gene encoding a conserved uncharacterized protein, EipB, is present in all sequenced *Brucella* and several other genera in the class *Alphaproteobacteria.* To our knowledge, this study presents the first functional and structural characterization of a protein from the DUF1849 family, to which

55 EipB belongs. EipB is secreted to the periplasm where it forms a spiral-like anti-parallel β
56 structure. Deletion of *Brucella eipB* results in defects of the cell envelope and in reduced
57 virulence in an animal model of disease. *eipB* genetically interacts with *ttpA*, which also
58 encodes a periplasmic protein. We propose that EipB and TtpA function as part of a
59 system required for cell envelope homeostasis in select *Alphaproteobacteria*.
60

61 # Introduction

62 *Brucella* spp. are the causative agents of brucellosis, which afflicts wildlife and livestock on
63 a global scale and can occur in humans through contact with infected animals or animal
64 products (1, 2). These intracellular pathogens are members of the class
65 *Alphaproteobacteria*, a group of Gram-negative species that exhibit tremendous diversity
66 in metabolic capacity, cell morphology, and ecological niches (3). In their mammalian
67 hosts, *Brucella* cells must contend with the host immune system (4) and adapt to stresses
68 including oxidative assault from immune cells, acidic pH in the phagosomal compartment,
69 and nutrient shifts during intracellular trafficking (5). Molecular components of the cell
70 envelope play a key role in the ability of *Brucella* spp. to survive these stresses and to
71 replicate in the intracellular niche (6, 7). As part of a systematic experimental survey of
72 conserved *Alphaproteobacterial* protein **d**omains of **u**nknown **f**unction (DUFs), we recently
73 described **e**nvelope **i**ntegrity **p**rotein **A** (EipA). This periplasmic protein confers resistance
74 to cell envelope stressors and determines *B. abortus* virulence in a mouse model of
75 infection (8). In this study, we report a functional and structural analysis of **e**nvelope
76 **i**ntegrity **p**rotein **B** (EipB), a member of the uncharacterized gene family DUF1849.
77

78 DUF1849 (Pfam: PF08904) is almost entirely restricted to the *Alphaproteobacteria* (9).
79 Within this taxonomic class, it is widespread among the *Rhizobiales*, *Rhodospirillales* and
80 *Rhodobacterales* (Figure 1). To our knowledge, no functional data have been reported for
81 this gene family other than results from a recent multi-species Tn-seq study that showed
82 stress sensitivity in *Sinorhizobium meliloti* strains harboring transposon insertions in the
83 DUF1849 gene, *SMc02102* (10). Here we show that in *Brucella*, the DUF1849 protein EipB
84 (locus tag *bab1_1186*; RefSeq locus BAB_RS21600) is a 280-residue periplasmic protein
85 that folds into a 14-stranded, open β-barrel containing a conserved disulfide bond. We
86 term this novel barrel structure a β-spiral and show that it resembles the lipoprotein
87 chaperone LolB, though its overall fold is distinct. Replication and survival of a *B. abortus*
88 strain in which we deleted *eipB* was attenuated in a mouse infection model, and deletion of
89 *eipB* in both *B. abortus* and *Brucella ovis* enhanced sensitivity to compounds that affect the
90 integrity of the cell envelope. We have further shown that *B. abortus eipB* deletion is
91 synthetically lethal with transposon disruption of *bab1_0430*, which encodes a periplasmic
92 **t**etratrico**p**eptide-**r**epeat (TPR) protein that we have named TtpA. The *Brucella melitensis*
93 ortholog of TtpA (locus tag BMEI1531) has been previously described as a molecular
94 determinant of mouse spleen colonization (11), while a *Rhizobium leguminosarum* TtpA
95 homolog (locus tag RL0936) is required for proper cell envelope function (12). We propose
96 that TtpA and EipB coordinately function in the *Brucella* periplasm to ensure cell envelope
97 integrity and to enable cell survival in the mammalian host niche.

98

99 # Results

100 ### ***B. abortus eipB* is required for maintenance of mouse spleen colonization**

101 As part of a screen to evaluate the role of conserved *Alphaproteobacterial* genes of
102 unknown function in *B. abortus* infection biology, we infected THP-1 macrophage-like cells
103 with wild-type *B. abortus*, an *eipB* deletion strain (Δ*eipB*), and a genetically complemented
104 Δ*eipB* strain. Infected macrophages were lysed and colony forming units (CFU) were
105 enumerated on tryptic soy agar plates (TSA) at 1, 24 and 48 hours post-infection. We
106 observed no significant differences at 1, 24 or 48 hours post-infection, indicating that *eipB*
107 was not required for entry, intracellular replication or survival *in vitro* (Figure 2A).
108
109 We further evaluated the role of *eipB* in a BALB/c mouse infection model. Mice infected
110 with Δ*eipB* had no significant difference in spleen weight or bacterial load compared to
111 mice infected with wild-type *B. abortus* strain 2308 at one-week post-infection (Figure 2B).
112 However, at 4- and 8-weeks post-infection, mice infected with the wild-type or the
113 complemented *eipB* deletion strains had pronounced splenomegaly and a bacterial load of
114 approximately 5 x 10^6 CFU/spleen. In contrast, mice infected with Δ*eipB* had smaller
115 spleens with approximately 2 orders fewer bacteria (~1 x 10^4 CFU/spleen) (Figure 2B). We
116 conclude that *eipB* is not required for initial spleen colonization but is necessary for full
117 virulence and persistence in the spleen over an 8-week time course.
118
119 To assess the pathology of mice infected with wild-type and Δ*eipB* strains, we harvested
120 spleens at 8 weeks post-infection and fixed, mounted, and subjected the samples to
121 hematoxylin and eosin (H&E) staining (Figure 3). Compared to naïve (uninfected) mice
122 (Figure 3A), we observed higher extramedullary hematopoiesis, histiocytic proliferation,
123 granulomas, and the presence of *Brucella* immunoreactivities in spleens of mice infected
124 with wild-type *B. abortus* 2308 and the genetically-complemented mutant strain (Figure 3B

125 and D). Both wild-type and the complemented strain caused spleen inflammation, with a
126 reduced white to red pulp ratio as a result of lymphoid follicle disruption and red pulp
127 expansion; these spleens also had increased marginal zones (Figure 3B and D). Mice
128 infected with Δ*eipB* had reduced pathologic features: there was minimal change in white to
129 red pulp ratio, and a minimal increase in marginal zones (Figure 3C). There was no
130 evidence of extramedullary hematopoiesis in mice infected with Δ*eipB*, though histiocytic
131 proliferation was mildly increased. Granulomas and *Brucella* immunoreactivities were rare
132 in Δ*eipB* (Figure 3C). These results are consistent with a model in which *eipB* is required
133 for full *B. abortus* virulence in a mouse model of infection. A summary of spleen pathology
134 scores is presented in Table S1.
135
136 We further measured antibody responses in mice infected with Δ*eipB* and wild-type strains.
137 Serum levels of total IgG, *Brucella*-specific IgG, IgG1, and IgG2a were measured by
138 enzyme-linked immunosorbent assays (ELISA) (Figure 2C-F). At 8 weeks post-infection,
139 total serum IgG was higher in all infected mice relative to the uninfected control (Figure
140 2C). The level of *Brucella*-specific IgG was approximately 6 times higher in Δ*eipB*-infected
141 mice than in mice infected with wild-type or the complemented mutant strain (Figure 2D).
142 Mice infected with wild-type, Δ*eipB* and the Δ*eipB*-complemented strain displayed similar
143 increases in IgG1 and IgG2a at 8 weeks post infection (Figure 2E and F). We conclude
144 that Δ*eipB* infection results in production of more *B. abortus*-specific antibodies. We did not
145 test whether these antibodies contribute to clearance of the Δ*eipB* strain. Antibody
146 production may simply be a consequence of antigen release triggered by host clearance of
147 Δ*eipB* by other immune mechanisms.
148

149 **The Δ*eipB* strain is sensitive to cell envelope stressors**

150 To test whether reduced virulence of Δ*eipB* correlates with an increased sensitivity to
151 stress *in vitro*, we evaluated *B. abortus* Δ*eipB* growth on TSA plates supplemented with
152 known cell membrane/envelope stressors including EDTA, ampicillin and deoxycholate.
153 Δ*eipB* had 1.5 to 3 logs fewer CFU compared to wild-type when titered on TSA plates
154 containing these compounds. All phenotypes were complemented by restoring the Δ*eipB*
155 locus to wild-type (Figure 4A). Together, these data provide evidence that *eipB* contributes
156 to resistance to compounds that compromise the integrity of the *B. abortus* cell
157 membrane/envelope.

158

159 Although Δ*eipB* CFUs were reduced relative to wild-type on agar plates containing all three
160 envelope stressors that we assayed, we observed no apparent defects in Δ*eipB* cell
161 morphology by light microscopy or cryo-electron microscopy when cultivated in liquid broth
162 (Figure 4B and C). Incubation of Δ*eipB* with 2 mM EDTA or 5 μg/ml ampicillin (final
163 concentration) in Brucella broth for 4 hours also had no apparent effect on cell structure,
164 nor did *eipA* overexpression (Figure 4B and C). Longer periods of growth in the presence
165 of stressors may be required for differences in cell morphology/structure to be evident in
166 broth. It may also be the case that the envelope stress phenotypes we observe are
167 particular to growth on solid medium.

168

169 ***B. abortus* Δ*eipB* agglutination phenotypes indicate the presence of smooth LPS**

170 In *B. abortus*, smooth LPS (containing O-polysaccharide) is an important virulence
171 determinant (13). Smooth LPS can also act as a protective layer against treatments that
172 compromise the integrity of the cell envelope (14). Loss of smooth LPS in *B. abortus* Δ*eipB*

173 could therefore explain the phenotypes we observe for this strain. To test this hypothesis,
174 we assayed wild-type and Δ*eipB* agglutination in the presence of serum from a *B. abortus*-
175 infected mouse. A major serological response to smooth *Brucella* species is to O-
176 polysaccharide (15), and thus agglutination can provide an indirect indication of the
177 presence or absence of smooth LPS on the surface of the cell. Both wild-type and Δ*eipB*
178 strains agglutinated in the presence of serum, providing evidence for the presence of O-
179 polysaccharide in Δ*eipB* (Figure 5A). As a negative control, we incubated the naturally
180 rough species *B. ovis* with mouse serum; *B. ovis* did not agglutinate in the presence of
181 serum (Figure 5A). We further assayed agglutination of *B. abortus* wild-type and Δ*eipB*
182 strains in the presence of acriflavine, which is demonstrated to agglutinate rough strains
183 such as *B. ovis* (16, 17). After 2 hours of incubation, we observed no agglutination of wild-
184 type *B. abortus* or Δ*eipB* (Figure 5B). We treated *B. ovis* with acriflavine as a positive
185 control and observed agglutination as expected (Figure 5B). Together, these data indicate
186 that deletion of *eipB* does not result in a loss of smooth LPS. However, we cannot rule out
187 the possibility that the chemical structure of O-polysaccharide is altered in Δ*eipB*.
188

189 **EipB is a monomeric protein that is secreted to the periplasm**

190 The N-terminus (residues M1-A30) of *Brucella* EipB contains a predicted signal peptide
191 based on SignalP 4.2 analysis (18). EipB (DUF1849) homologs in other
192 *Alphaproteobacteria* also have a predicted N-terminal secretion signal (Figure S1). We
193 note that EipB in our wild-type *B. abortus* 2308 strain has a methionine instead of a leucine
194 at position 250. These two amino acids are interchangeable at this position in DUF1849
195 (Figure S2). To test the prediction that EipB is a periplasmic protein, we fused the
196 *Escherichia coli* periplasmic alkaline phosphatase gene (*phoA*) to *B. abortus eipB* and

197 expressed fusions from a *lac* promoter in *B. ovis*. We generated (i) the full-length EipB
198 protein (M1-K280) fused at its C-terminus to *E. coli* PhoA (EipB-PhoA$_{Ec}$) and (ii) an EipA-
199 PhoA fusion lacking the hypothetical EipB signal peptide sequence (EipB$^{S29-K280}$-PhoA$_{Ec}$).
200 After overnight growth in Brucella broth in presence or absence of 1 mM isopropyl β-D-1-
201 thiogalactopyranoside (IPTG), we adjusted each culture to the same density and loaded
202 into a 96-well plate containing 5-bromo-4-chloro-3-indolyl phosphate (BCIP, final
203 concentration 200 µg/ml). BCIP is hydrolyzed to a blue pigment by PhoA, which can be
204 measured colorimetrically. BCIP diffusion through the inner membrane is inefficient, and
205 thus this reagent can be used to specifically detect PhoA activity in the periplasmic space
206 or in the extracellular medium (19). After a 2-hour incubation at 37°C, the well containing
207 the *B. ovis* cells expressing the EipB$^{M1-K280}$-PhoA$_{Ec}$ fusion turned dark blue. We observed
208 no color change in the well containing the *B. ovis* strain expressing the EipB$^{S29-K280}$-PhoA$_{Ec}$
209 protein fusion (Figure 6A). As expected, no color change was observed in absence of
210 induction with 1 mM IPTG (Figure 6A). To test if EipB is secreted from the cell into the
211 growth medium, we performed a similar experiment on spent medium supernatants from
212 the different cultures. We observed no color change in these samples after 2 hours of
213 incubation providing evidence that EipB$^{M1-K280}$-PhoA$_{Ec}$ is not secreted from the cell.
214
215 We further assayed the oligomeric state of affinity-purified *B. abortus* EipB in solution by
216 size-exclusion chromatography. The calculated molecular mass of His$_6$-EipB (V31-K280) is
217 30.7 kDa. This protein eluted from a sizing column at a volume with an apparent molecular
218 mass of ~23 kDa, which is consistent with a monomer (Figure 6B). There was no evidence
219 of larger oligomers by size-exclusion chromatography. From these data, we conclude that
220 EipB is likely a monomeric periplasmic protein.

221

222 **EipB folds into a spiral-like β-sheet that resembles PA1994, LolA and LolB**

223 We postulated that the three-dimensional structure of EipB may provide molecular-level
224 insight into its function in the cell. As such, we solved an x-ray crystal structure of *B.*
225 *abortus* EipB (residues A30-K280; PDB ID: 6NTR). EipB lacking its signal peptide formed
226 triclinic crystals (a=47.4 Å b=69.2 Å, c=83.2 Å, α=90.1, β=90.0°, γ=78.7°) that diffracted to
227 2.1 Å resolution; we refined this structure to R_{work}= 0.195 and R_{free}= 0.245. Crystallographic
228 data and refinement statistics are summarized in Table S2. Four EipB molecules (chains
229 A-D) are present in the crystallographic asymmetric unit.

230

231 Each EipB monomer consists of 14 antiparallel β-strands, with β1-β12 and β14-β15
232 forming an oval, spiral-like β-sheet (minor axis diameter: ~25 Å; major axis diameter: ~35
233 Å). Two regions of this β-spiral, involving β5, β6, β7, β8 and the hairpin loop connecting β9
234 and β10, overlap (Figure 7A and B). Interactions between these two overlapping portions
235 of structure are mostly hydrophobic, though polar contacts are also found in these regions
236 (Figure 8A and B). One side of the spiral is occluded by β-strand 13 and α-helix 2, forming
237 the bottom of this "cup" shaped protein. The external surface of EipB is positively and
238 negatively charged, and also presents small hydrophobic patches (Figure S3); two helices,
239 α1 (for which electron density is evident only in chains A and C) and α3, are positioned at
240 the surface of the cylindrical β-spiral (Figure 7A and B). The lumen of EipB is solvent
241 accessible and is partially filled with the side chains of hydrophobic or acidic residues.
242 Hydrophobic residues represent ~52% of the residues present inside the EipB cavity
243 (Figure 7 and 8). The size of this cavity suggests that EipB, in this conformation, can
244 accommodate small molecules or ligands in its lumen.

245

246 We searched the Dali database (20) with the EipB structure, but failed to identify clear
247 structural homologs. *Pseudomonas aeruginosa* PA1994 (PDB ID: 2H1T) (21) was the
248 closest structural match to EipB (RMSD ~3.5; Z-score ~11) (Figure S4A). Despite very low
249 sequence identity (~8%), PA1994 has noticeable structural similarities to EipB: it adopts a
250 spiral-like β-fold involving 15 β-strands, which is occluded at one end with a long α-helix.
251 Unlike EipB, PA1994 lacks a signal peptide and is predicted to be a cytoplasmic protein.
252 Structural parallels between PA1994 and the periplasmic lipoprotein chaperones LolA/LolB
253 have been noted and a role for PA1994 in glycolipid metabolism has been postulated (21),
254 though this prediction remains untested. Like PA1994, EipB has structural similarities to
255 LolA and LolB, in particular the antiparallel and curved β-sheet scaffold that engulfs a
256 central α-helical plug (Figure S4B). Whether *Brucella* EipB, or DUF1849 proteins more
257 generally, function in trafficking lipoproteins or other molecules in the periplasm also
258 remains to be tested.

259

260 **EipB has a conserved disulfide bond**

261 We identified two cysteines in EipB, C69 and C278, which are the two most conserved
262 residues in the DUF1849 sequence family (Figures S1 and S2). C69 is solvent exposed in
263 *Brucella* EipB and positioned in a loop connecting β2 and β3. C278 is present at the C-
264 terminus of the protein, which immediately follows β15. β15 interacts with β14 and β1, and
265 is spatially proximal to β2 and β3 (Figure 9A). Given the proximity of these two cysteines in
266 the EipB structure, we hypothesized that C69 and C278 could form an internal disulfide
267 bond. However, electron density for the 10 C-terminal residues (containing C278) is not
268 well resolved in the crystal structure, and a disulfide bond is not evident, likely because the

269 protein was dialyzed against a buffer containing 2 mM 1,4-dithiothreitol (DTT) prior to
270 crystallization.
271
272 To biochemically test if these two cysteines form a disulfide bond, we purified *B. abortus*
273 EipB under non-reducing conditions and mixed the protein with SDS gel loading dye with
274 and without 1 mM DTT. We observed two bands that migrated differently in the 30 kDa
275 region when the protein was resolved by 12% SDS-PAGE. EipB incubated with DTT
276 migrated farther than the untreated protein, suggesting the presence of a disulfide bond
277 (Figure 9B). We performed this same experiment with three different EipB cysteine mutant
278 proteins in which C69, C278, or both were mutated to serine. In the absence of DTT,
279 $EipB^{C69S}$ and $EipB^{C278S}$ migrated at an apparent molecular weight of ~60 kDa,
280 corresponding to a dimeric EipB interacting through an S-S bond. After DTT treatment,
281 these mutant proteins migrated the same as the reduced wild-type protein (Figure 9B). As
282 expected, the double cysteine mutant ($EipB^{C69S+C278S}$) did not form an apparent dimer and
283 was unaffected by DTT (Figure 9B). From these data, we conclude that an internal
284 disulfide bond can form between C69 and C278 in EipB and is likely present *in vivo*, as
285 EipB resides in the oxidizing environment of the periplasm.
286
287 To test whether this disulfide bond affects EipB function, we measured CFU of a *Brucella*
288 *ovis* Δ*eipB* strain expressing wild-type *B. abortus* EipB or cysteine disulfide mutants on
289 agar plates containing 3 µg/ml carbenicillin. *B. ovis* is a closely related biosafety level 2
290 (BSL2) surrogate for *B. abortus*. *B. ovis* and *B. abortus* EipB are identical with the
291 exception of one amino acid at position 250 (Figure S2). In this carbenicillin assay (Figure
292 9C and D), *B. abortus* EipB complemented a *B. ovis* Δ*eipB* strain, suggesting that the

293 substitution at residue 250 does not impair EipB function. We placed four different versions
294 of *eipA* under the control of a *lac* promoter (P_{lac}): P_{lac}-*eipB*^{WT}, P_{lac}-*eipB*^{C69S}, P_{lac}-*eipB*^{C278S},
295 and P_{lac}-*eipB*$^{C69S+C278S}$; the empty vector was used as a control. After 5 to 6 days of growth
296 on Schaedler Blood Agar (SBA) containing 3 µg/ml of carbenicillin and no IPTG, we
297 observed poor growth at only the lowest dilution for wild-type and Δ*eipB* strains carrying
298 the empty vector control. Corresponding colonies for strains carrying the different P_{lac}-*eipB*
299 overexpression plasmids were more abundant though very small in the absence of IPTG
300 induction. However, the strain harboring the wild-type *eipB* plasmid systematically grew at
301 1 log higher dilution than the cysteine mutant strains indicating that the presence of the
302 disulfide bond in *eipB* contributes to carbenicillin resistance on solid medium (Figure 9C
303 and D, see also Figure S5A). These results indicate some level of leaky expression from
304 the multi-copy P_{lac}-*eipA* plasmids. When induced with IPTG, overexpression of the
305 different EipB variants enhanced growth in all strains. (Figure 9C and D). As expected,
306 strains grown on control plates without carbenicillin had no growth defect, with or without
307 IPTG induction (Figure 9D). *B. ovis* Δ*eipB* strains expressing the different variants of *eipB*
308 appeared normal by phase contrast microscopy (see Figure S5B). These results provide
309 evidence that EipB is necessary for full carbenicillin resistance in *B. ovis*, and that
310 cysteines 69 and 278 contribute to EipB function *in vivo*.
311
312 To evaluate the effect of these two cysteines on EipB stability *in vitro*, we measured the
313 thermal stability of purified wild-type *B. abortus* EipB (EipB^{WT}) and double cysteine mutant
314 (EipB$^{C692+C278S}$) in presence or absence of 2 mM DTT. EipB^{WT} melted at ~46°C in absence
315 of DTT and at ~41.5°C in presence of DTT. EipB$^{C692+C278S}$ melted at ~42.3°C in the
316 presence or absence of DTT (see Figure S6). We conclude that an internal disulfide bond

317 stabilizes EipB structure *in vitro*. Reduced stability of EipB lacking its conserved disulfide
318 bond may explain the 1 log relative growth defect of Δ*eipB* strains expressing EipB
319 cysteine mutants on SBA carbenicillin (Figure 9C and D).
320
321 ***eipB* deletion is synthetically lethal with *bab1_0430* (*ttpA*) disruption, and**
322 **synthetically sick with disruption of multiple genes with cell envelope functions**
323 To further characterize how *eipB* functions in the *Brucella* cell, we aimed to identify
324 transposon (Tn) insertion mutations that are synthetically lethal with *eipB* deletion in *B.*
325 *abortus* (see Tables S3 and S4). In other words, we sought to discover genes that are
326 dispensable in a wild-type genetic background, but that cannot be disrupted in a Δ*eipB*
327 background. By sequencing a Tn-Himar insertion library generated in *B. abortus* Δ*eipB*
328 (NCBI Sequence Read Archive accession SRR8322167) and a Tn-Himar library generated
329 in wild-type *B. abortus* (NCBI Sequence Read Archive accession SRR7943723), we
330 uncovered evidence that disruption of *bab1_0430* (RefSeq locus BAB_RS17965) is
331 synthetically lethal with *eipB* deletion. Specifically, reproducible reads corresponding to
332 insertions in the central 10-90% of *bab1_0430* were not evident in Δ*eipB*, but were present
333 in wild type (Figure 10A). *bab1_0430* encodes a 621-residue **t**etratrico**p**eptide **r**epeat-
334 containing (TPR) protein that contains a predicted signal peptide and signal peptidase site
335 at its N-terminus. This protein was previously detected by mass spectrometry analyses of
336 *B. abortus* extracts, and described as a cell-envelope associated (22), or periplasmic
337 protein (23). Hereafter, we refer to this gene as *ttpA* based on its similarity to *R.*
338 *leguminosarum ttpA* (12).
339

340 Genes involved in LPS O-antigen synthesis, and previously described as synthetic lethal
341 with *eipA* (*bab1_1612*) deletion in *B. abortus* (8), were synthetic sick with *eipB* deletion
342 (Figure 10A), as were genes involved in peptidoglycan synthesis: *mltA* (*bab1_2076*, lytic
343 murein transglycosylase A) and *bab1_0607* (glycosyl transferase/penicillin-binding protein)
344 (24) (Figure 10A). There were reduced transposon insertions in solute binding protein
345 *yejA1* (*bab1_0010*) (Figure 10A), which is involved in *B. melitensis* resistance to polymyxin
346 (25). *lnt* (*bab1_2158*) and *vltR* (*bab1_1517*) were also synthetic sick with Δ*eipB*. *lnt* is an
347 apolipoprotein N-acyltransferase involved in lipoprotein synthesis (26); *vltR* encodes a
348 LysR transcriptional regulator required for full *B. abortus* virulence (27) (Figure 10A).
349 Finally, the general stress sensor kinase *lovHK* (*bab1_0652*) (28), *bab1_1293* (homoserine
350 dehydrogenase), and *bab1_0188* (methionine synthase), had fewer Tn insertions in the
351 Δ*eipB* background relative to wild type (Figure 10A).
352
353 ***ttpA contributes to carbenicillin resistance***
354 Transposon insertions in *ttpA* were the most detrimental insertions in a Δ*eipB* background,
355 so we chose to further characterize this gene. All efforts to delete *B. ovis ttpA* (locus tag
356 *bov_0411*) using a classic crossover recombination and *sacB* counterselection approach
357 were unsuccessful, though hundreds of clones were screened. Efforts to delete the
358 chromosomal copy by expressing a copy of *ttpA* from a plasmid also failed. This result is
359 surprising considering that transposon insertions in *B. abortus ttpA* (NCBI Sequence Read
360 Archive accession SRR7943723) and *B. ovis ttpA* (NCBI Sequence Read Archive
361 accession SRR7943724) are tolerated (8). As an alternative approach to study the function
362 of this gene, we inactivated *ttpA* using a single crossover recombination strategy. The
363 corresponding *B. ovis* strain (Δ*ttpA*) was then transformed with a plasmid-borne IPTG-

364 inducible copy of *ttpA* (pSRK-*ttpA*) or with an empty plasmid vector (EV). We evaluated
365 sensitivity of these strains to carbenicillin by plating a dilution series on SBA plates
366 containing 2.5 µg/ml carbenicillin, with or without IPTG inducer (Figure 10B and 10C).
367 When compared to wild-type with empty vector, *B. ovis* Δ*ttpA* with empty vector had ~0.5
368 log reduced CFU on carbenicillin SBA. The corresponding colonies of *B. ovis* Δ*ttpA* were
369 noticeably smaller than wild-type. Genetic complementation of Δ*ttpA* with pSRK-*ttpA*
370 restored growth on carbenicillin plates. *B. ovis* Δ*ttpA*/pSRK-*ttpA* had ~1.5 log more
371 colonies than wild-type in the presence of carbenicillin, with or without IPTG induction.
372 Thus, leaky expression of *ttpA* from the *lac* promoter on pSRK-*ttpA* is apparently sufficient
373 to protect this strain from carbenicillin on solid medium. Morphology of the *B. ovis* Δ*ttpA*
374 strains appeared normal by phase contrast microscopy at 630x magnification (Figure S7).
375
376 To further evaluate the effect of *ttpA* overexpression, we assayed *B. ovis* wild-type and
377 Δ*eipB* strains carrying pSRK-*ttpA*. As before, we tested sensitivity of these inducible
378 expression strains to carbenicillin by plating a dilution series on SBA plates containing 3
379 µg/ml of carbenicillin, with or without 2 mM IPTG inducer (Figure 11A and B). Wild-type *B.*
380 *ovis*/pSRK-*ttpA* and wild-type *B. ovis*/pSRK-*eipB* strains had equivalent CFU in the
381 absence of carbenicillin, with or without IPTG. *ttpA* or *eipB* provided a ~3 log protective
382 effect without IPTG induction in the presence of carbenicillin compared to the wild-type
383 empty vector strain (Figure 11). Surprisingly, inducing *ttpA* expression with IPTG reduced
384 its protective effect by 1 log on carbenicillin (relative to uninduced), and the corresponding
385 colonies were very small suggesting slower growth under this condition (Figure 11B and
386 C). This may be an effect of IPTG, based on reduced CFU counts of wild-type empty
387 vector control under this condition. As expected, induced expression of *eipB* from P_{lac}-*eipB*

388 rescued the carbenicillin viability defect of Δ*eipB*. However, induced expression of *ttpA*
389 from P_{lac}-*ttpA* was not sufficient to rescue the Δ*eipB* carbenicillin phenotype (Figure 11B
390 and C). As before, we observed highly reduced CFU for *B. ovi*s wild-type or Δ*eipB* control
391 strains carrying the pSRK empty vector (EV), when challenged with 3 µg/ml of
392 carbenicillin. Morphology of wild-type or Δ*eipB B. ovis* strains overexpressing *ttpA*
393 appeared normal by phase contrast microscopy at 630x magnification (Figure S8).
394
395 The observed genetic interaction between *eipB* and *ttpA* raised the possibility that their
396 gene products physically interact. We tested interaction between EipB and TtpA proteins
397 using bacterial two-hybrid and biochemical pull-down assays. We further evaluated
398 whether a possible EipB-TtpA interaction is influenced by the presence or absence of the
399 EipB internal disulfide bond using a biochemical pull-down. For our bacterial two-hybrid
400 assay, $EipB^{V31-K280}$ was fused to the T25 adenylate cyclase fragment, and $TtpA^{K31-D621}$ was
401 fused to the T18 or T18C adenylate cyclase fragments. For the pull-down assay, MBP-
402 tagged TtpA (K31-D621) and His-tagged EipB (V31-K280; wild-type and the different
403 cysteine mutants) were co-purified in presence or absence of DTT. We found no evidence
404 for direct interaction between EipB and TtpA, suggesting that the function of these two
405 proteins in *Brucella* envelope stress adaptation is not achieved through direct interaction
406 (Figure S9).
407
408 **DISCUSSION**
409 Bacterial genome sequencing efforts over the past two decades have revealed thousands
410 of protein domains of unknown function (DUFs). The DUF1849 sequence family is
411 prevalent in orders *Rhizobiales*, *Rhodobacterales* and *Rhodospirillales* in the

412 *Alphaproteobacteria*. To date, the function of this domain has remained undefined. In this
413 study, we have shown that a DUF1849 gene in *Brucella* spp., named *eipB*, encodes a 14-
414 stranded β-spiral protein that is secreted to the periplasm and that contains a conserved
415 disulfide bond (Figures 9, S1 and S2). *eipB* is required for maintenance of *B. abortus*
416 spleen colonization in a mouse model of infection (Figure 2), and *eipA* deletion in *B.*
417 *abortus* and in *B. ovis* results in sensitivity to treatments that compromise the integrity of
418 the cell envelope *in vitro* (Figure 3). Envelope stress sensitivity of the *B. abortus* Δ*eipB*
419 mutant likely contributes to its reduced virulence in a mouse.
420
421 *A lipoprotein connection?*
422 An x-ray crystal structure of EipB shows that this periplasmic protein adopts an unusual β-
423 spiral fold that shares structural similarity (DALI Z-score= 11.0) with a functionally-
424 uncharacterized *P. aeruginosa* protein, PA1994, despite low sequence homology (Figure
425 S4). It was previously noted that PA1994 has structural features that resemble the
426 lipoprotein carrier and chaperone proteins LolA and LolB (21), which have a central role in
427 lipoprotein localization in select Gram-negative bacteria (29). Like LolA, LolB, and PA1994,
428 *Brucella* EipB forms a curved hydrophobic β-sheet that is wrapped around an α-helix
429 (Figure S4B). Homologs of LolA are present in *Brucella* and other *Alphaproteobacteria*, but
430 homologs of LolB are missing (26). Given the EipB structure, its periplasmic localization,
431 and the phenotypes of a Δ*eipB* deletion strain it is tempting to speculate that EipB
432 (DUF1849) has a LolB-like function in the *Brucella* cell. However, it seems unlikely that
433 LolB and EipB function in a structurally- or biochemically-equivalent manner. Certainly, we
434 observe surface-level similarity between LolA/LolB and EipB structures (Figure S4),
435 particularly in the antiparallel β-sheet region, but these proteins have topological

436 differences that distinguish their folds. Moreover, LolB is a membrane anchored lipoprotein
437 that facilitates lipoprotein targeting at the inner leaflet of the outer membrane. In contrast,
438 *Brucella* EipB does not have a predicted site for lipidation (i.e. a lipobox), and is therefore
439 unlikely to function as a membrane-anchored protein.
440
441 The number of uniquely barcoded Tn-Himar insertions in the apolipoprotein N-
442 acyltransferase *lnt* (*bab1_2158*; *lnt* conserved domain database score < e^{-173}) is lower than
443 expected in a Δ*eipB* background relative to wild-type (Figure 10A). This provides indirect
444 evidence for a link between *eipB* and lipoproteins. Lnt catalyzes the final acylation step in
445 lipoprotein biogenesis (30), which is often considered to be an essential biochemical
446 process. However, like *Francisella tularensis* and *Neisseria gonorrhoeae* (31), *B. abortus*
447 *lnt* is dispensable (24) (Figure 10A and Table S4). The data presented here suggest that
448 transposon insertions are less tolerated in *B. abortus lnt* when *eipB* is missing. Additional
449 experimentation is required to test a possible functional relationship between *lnt* and *eipB*.
450 However, it is notable that we did not observe a synthetic genetic interaction between *lnt*
451 and the gene encoding the structurally-unrelated periplasmic envelope integrity protein,
452 EipA, in a parallel Tn-seq experiment (8). Whether *eipB* actually influences lipoprotein
453 biogenesis or localization remains to be tested.
454
455 *TtpA: a periplasmic determinant of cell envelope function in Rhizobiaceae*
456 Transposon disruption of *ttpA* (*bab1_0430*) is not tolerated when *eipB* is deleted. Though
457 there is a genetic interaction between *eipB* and *ttpA*, we found no evidence for a direct
458 physical interaction between these two periplasmic proteins (Figure S9). Like *eipB*, *ttpA*
459 influences *in vitro* sensitivity to carbenicillin (Figure 10B and C). TtpA contains a TPR

460 motif. In bacteria, TPR proteins function in many different pathways including cell envelope
461 biogenesis, and are often molecular determinants of virulence (32, 33). Deletion of *ttpA*
462 attenuates *B. melitentis* virulence in a mouse infection model (11) and increases *R.*
463 *leguminosarum* membrane permeability and sensitivity to SDS and hydrophobic antibiotics
464 (12), respectively. A genetic interaction between *ttpA* and the **c**omplex **m**edia growth
465 **d**eficiency (*cmdA-cmdD*) operon has been reported in *R. leguminosarum*. Mutations in this
466 operon result in envelope dysfunction and defects in cell morphology (12, 34). While *B.*
467 *abortus* contains a predicted *cmd* operon (*bab1_1530, bab1_1531, bab1_1532, and*
468 *bab1_1533*) these genes remain uncharacterized. We found no evidence for a synthetic
469 genetic interaction between *eipB* and *cmd* in *B. abortus*, nor has such an interaction
470 between *eipB* orthologs and *cmd* been reported in other *Rhizobiaceae*.
471
472 Notably, leaky expression of either *eipB* or *ttpA* from a plasmid strongly protected *B. ovis*
473 from a cell wall antibiotic (carbenicillin). In the wild-type *B. ovis* background, we observed a
474 phenomenon in which induced *ttpA* overexpression resulted in less protection against
475 carbenicillin than low-level (leaky) expression (Figure 11A and B). Induced expression of
476 *eipB* from a plasmid did not have this parabolic effect on cell growth/survival in the face of
477 carbenicillin treatment. Considering that EipB and TtpA confer resistance to ampicillin and
478 carbenicillin, two β-lactam antibiotics that inhibit synthesis of the peptidoglycan, one might
479 hypothesize that these proteins influence the structure or synthesis of the cell wall. This
480 hypothesis is reinforced by the fact that a lytic murein transglycosylase and a class A
481 PBP/glycosyl transferase were found to be synthetic sick with *eipB* deletion (Figure 10A).
482 In *E. coli*, the TPR containing protein LpoA is proposed to reach from the outer membrane
483 through the periplasm to interact with the peptidoglycan synthase PBP1A (35). Models in

484 which EipB affects lipoprotein biosynthesis and/or cell wall metabolism are important to
485 test as we work toward understanding how *eipB* functions to ensure *Brucella* cell envelope
486 integrity and survival in a mammalian host.

487
488

489 Materials and Methods

490 Agglutination assays, mouse and macrophage infection assays and the transposon
491 sequencing experiments for this study were performed in parallel with our recent studies of
492 *eipA* (8).

493

494 All experiments using live *B. abortus* 2308 were performed in Biosafety Level 3 facilities
495 according to United States Centers for Disease Control (CDC) select agent regulations at
496 the University of Chicago Howard Taylor Ricketts Laboratory. All the *B. abortus* and *B. ovis*
497 strains were cultivated at 37°C with 5% CO_2; primer and strain information is available in
498 Table S5.

499

500 Chromosomal deletions in *B. abortus* and in *B. ovis*

501 The *B. abortus and B. ovis* Δ*eipB* deletion strains were generated using a double
502 recombination strategy as previously described (8). Briefly, fragments corresponding to the
503 500 base pair upstream region of *eipB* start codon and the 500 base pair downstream
504 region of *eipB* stop codon were ligated into the suicide plasmid pNPTS138 which carries
505 the *nptI* gene for initial kanamycin selection and the *sacB* gene for counter-selection on
506 sucrose. Genetic complementation of the *B. abortus* deletion strain was carried out by

507 transforming this strain with the pNPTS138 plasmid carrying the wild-type allele locus. The
508 *B. ovis* Δ*eipB* strain was complemented with the pSRK-*eipB* plasmid (IPTG inducible).
509
510 To inactivate *ttpA* in *B. ovis* (*bov_0411*), a 527-nucleotide long internal fragment was
511 cloned into pNPTS138-*cam* (a suicide plasmid that we engineered to carry a
512 chloramphenicol resistance marker) and used to disrupt the target gene by single
513 crossover insertion. The recombinant clones were selected on SBA plates supplemented
514 with 3 µg/ml chloramphenicol. This Δ*ttpA* strain was then complemented with pSRK-*ttpA*.
515
516 ***Brucella* EipB and TtpA overexpression strains**
517 For ectopic expression of *B. ovis* TtpA and the different versions of *B. abortus* EipB (wild-
518 type, cysteine mutants, and the EipB-PhoA$_{Ec}$ fusion with or without the signal peptide), the
519 pSRKKm (Kan^{R}) IPTG inducible plasmid was used (36). An overlapping PCR strategy was
520 used to introduce cysteine mutations and to stitch the different DNA fragments to the *E.*
521 *coli* alkaline phosphatase *phoA* (lacking its signal peptide). A Gibson-assembly cloning
522 strategy was then used to insert the different DNA fragments in the linearized pSRK
523 plasmid. After sequencing, plasmids were introduced in *B. abortus* or *B. ovis* by overnight
524 mating with *E. coli* WM3064 in presence of 300 µM of diaminopimelic acid (DAP) and
525 plated on SBA plates supplemented with kanamycin.
526
527 **Building and mapping the wild-type *B. abortus* and *B. abortus* Δ*eipB* Tn-Himar**
528 **insertion libraries**
529 To build and map the different Tn-Himar insertion libraries, we used a barcoded
530 transposon mutagenesis strategy developed by Wetmore and colleagues (37). A full and

531 detailed protocol can be found in our previous paper (8). Statistics for the two different
532 transposon insertion libraries are reported in Table S3. For each Himar insertion library,
533 Tn-seq read data have been deposited in the NCBI sequence read archive: *B. abortus*
534 2308 wild-type (BioProject PRJNA493942; SRR7943723), *B. abortus* Δ*eipB* (Δ*bab1_1186*)
535 (BioProject PRJNA510139; SRR8322167).
536
537 **Cell culture and macrophage infection assay**
538 Infection of inactivated macrophages differentiated from human monocytic THP-1 cells
539 were performed as previously described (8). Briefly, for infection assays, 5 x 10^6 *B. abortus*
540 cells were used to infect 5 x 10^4 THP-1 cells (multiplicity of infection of 1:100). To
541 determine the numbers of intracellular bacteria at 1, 24 and 48 hours post-infection, the
542 infected cells were lysed, the lysate was then serially diluted (10-fold serial dilution) and
543 plated on TSA plates to enumerate CFU.
544
545 **Mouse infection assay**
546 All mouse studies were approved by the University of Chicago Institutional Animal Care
547 and Use Committee (IACUC) and were performed as previously published (8). Briefly, 100
548 µl of a 5 x 10^5 CFU/ml *B. abortus* suspension were intraperitoneally injected into 6-week-
549 old female BALB/c mice (Harlan Laboratories, Inc.). At 1, 4, and 8 weeks post-infection, 5
550 mice per strain were sacrificed, and spleens were removed for weighing and CFU
551 counting. At week 8, blood was also collected by cardiac-puncture and serum from each
552 mouse was separated from blood using a serum separation tube (Sarstedt). Sera were
553 subsequently used for Enzyme-Linked ImmunoSorbent Assays (ELISA).
554

555 **Determination of antibody responses at 8 weeks post infection**

556 Total mouse serum IgG, IgG1, and IgG2a titers were measured using mouse-specific
557 ELISA kits by following manufacturer's instructions (eBioscience). *Brucella*-specific IgG
558 titers were determined as previously published (8).

559

560 **Spleen histology**

561 At 8 weeks post infection, spleens (n= 1 per strain) were prepared for histology as
562 previously described (8). Briefly, spleens were first fixed with formalin and submitted for
563 tissue embedding, Hematoxylin and Eosin (H & E) staining, and immunohistochemistry to
564 Nationwide Histology (Veradale, Washington). For immunohistochemistry, goat anti-
565 *Brucella* IgG was used (Tetracore, Inc). Pictures of fixed mouse spleen slides were
566 subsequently analyzed and scored.

567

568 **Plate stress assays**

569 Stress assays were performed as previously published (8). Briefly, the different *B. abortus*
570 and *B. ovis* strains were resuspended in sterile PBS or Brucella broth to an OD_{600} of ~
571 0.015 (~ 1 x 10^8 CFU ml^{-1}) and serially diluted (10-fold serial dilution). 5 µl of each dilution
572 were then spotted on TSA or SBA plates containing the different membrane stressors (2 to
573 5 µg/ml of ampicillin or carbenicillin, 200 µg/ml of deoxycholate or 2 mM EDTA).

574

575 To grow *B. ovis* strains containing pSRK-derived plasmids, all liquid cultures and plates
576 were supplemented with 50 µg/ml kanamycin. When necessary, 2 mM of IPTG was added
577 to the plates to induce ectopic expression of EipB or TtpA from pSRK. It is also important
578 to note that the *B. ovis* Δ*ttpA* strains carry the pNPTS138 suicide plasmid (used for gene

579 disruption) and are chloramphenicol resistant. However, no chloramphenicol was added to
580 the overnight cultures or the stress plates. For carbenicillin growth/survival assays, strains
581 were grown for 3 days at 37°C/ 5% CO_2 on SBA plates without carbenicillin, and for 5 to 6
582 days when these plates contained 2, 2.5 or 3 µg/ml of carbenicillin.
583

584 **Cryo-electron microscopy**

585 Cryo-electron microscopy was performed as previously described (8). Briefly, *B. abortus*
586 cultures in Brucella broth (OD_{600} of ~0.015) were prepared with 2 mM EDTA or ampicillin
587 (5 µg/ml) (final concentrations). After 4 hours of incubation in the presence of EDTA or
588 ampicillin, cells were harvested and fixed in PBS + 4% formaldehyde. After 1 hour, cells
589 were pelleted and resuspended in 500 µl EM buffer (38). Per CDC guidelines, cell killing
590 was confirmed before sample removal for imaging. Fixed *Brucella* cells were vitrified on
591 glow-discharged 200 mesh copper EM-grids with extra thick R2/2 holey carbon film
592 (Quantifoil). Per grid, 3 µl of the sample was applied and automatically blotted and plunged
593 into liquid ethane with the Leica EM GP plunge-freezer. Images were collected on a Talos
594 L120C TEM (Thermo Fischer) using the Gatan cryo-TEM (626) holder. The images were
595 acquired at a defocus between 8-10 µm, with a pixel size of 0.458 nm.
596

597 **Light microscopy images**

598 Phase-contrast images of *B. abortus* and *B. ovis* cells from plates or liquid broth (plus or
599 minus 1 mM IPTG) were collected using a Leica DM 5000B microscope with an HCX PL
600 APO 63×/1.4 NA Ph3 objective. Images were acquired with a mounted Orca-ER digital
601 camera (Hamamatsu) controlled by the Image-Pro software suite (Media Cybernetics). To

602 prepare the different samples, cells were resuspended in PBS containing 4%
603 formaldehyde.
604
605 **Agglutination assay**
606 Agglutination assays were performed as previously described (8). The different *Brucella*
607 strains (*B. ovis* and *B. abortus*) were harvested and resuspended in sterile PBS at OD_{600} ~
608 0.5. One milliliter of each cell suspension was loaded in a spectrophotometer cuvette and
609 mixed with 20 µl of wild-type *B. abortus*-infected mouse serum or with acriflavine (final
610 concentration 5 mM) and ODs were measured at 600 nm at time (0) and after 2 hours. As
611 a control, 1 ml of each cell suspension was also kept in a spectrophotometer cuvette
612 without serum or acriflavine.
613
614 **EipB expression, purification and crystallization**
615 The DNA fragment corresponding to the *B. abortus* EipB protein (residues 31 - 280) was
616 cloned into the pMCSG68 plasmid using a protocol previously published (8). For protein
617 expression, an *E. coli* BL21-Gold(DE3) strain was used. Seleno-methionine protein
618 expression and purification was performed as described (8). The purified protein was then
619 dialyzed against 20 mM HEPES, pH 8.0, 250 mM NaCl, and 2 mM DTT buffer and its
620 concentration was determined. The purified Se-Met EipB protein was concentrated to 160
621 mg/ml for crystallization. Initial crystallization screening was carried out using the sitting-
622 drop, vapor-diffusion technique. After a week, EipB crystallized in the triclinic space group
623 P1 from the condition #70 of the MCSG-2 crystallization kit that contains 25% PEG1500
624 and 20% glycerol. Prior to flash freezing in liquid nitrogen, crystals were cryo-protected by
625 briefly washing them in the crystallization solution containing 25% glycerol.

626

627 **Crystallographic data collection and data processing**

628 Se-Met crystal diffraction was measured at a temperature of 100 K using a 2-second
629 exposure/degree of rotation and was collected for 260°. Crystals diffracted to a resolution
630 of 2.1 Å and the corresponding diffraction images were collected on the ADSC Q315r
631 detector with an X-ray wavelength near the selenium edge of 12.66 keV (0.97929 Å) for
632 SAD phasing at the 19-ID beamline (SBC-CAT, Advanced Photon Source, Argonne,
633 Illinois). Diffraction data were processed using the HKL3000 suite (39). *B. abortus* EipB
634 crystals were twinned and the data had to be reprocessed and scaled from the $P2_1$ space
635 group to the lower symmetry space group P1 with the following cell dimensions: a= 47.36
636 Å, b= 69.24 Å, c= 83.24 Å, and α= 90.09°, β= 90.02°, γ= 78.66° (see Table S2). The
637 structure was determined by SAD phasing using SHELX C/D/E, mlphare, and dm, and
638 initial automatic protein model building with Buccaneer software, all implemented in the
639 HKL3000 software package (39). The initial model was manually adjusted using COOT
640 (40) and iteratively refined using COOT, PHENIX (41), and/or REFMAC (42); 5% of the
641 total reflections was kept out of the refinement in both REFMAC and PHENIX throughout
642 the refinement. The final structure converged to an R_{work} of 19.5% and R_{free} of 24.5% and
643 includes four protein chains (A: 30-270, B: 31-271, C: 30-271, and D: 30-270), 9 ethylene
644 glycol molecules, two glycerol molecules, and 129 ordered water molecules. The EipB
645 protein contained three N-terminal residues (Ser-Asn-Ala) that remain from the cleaved
646 tag. The stereochemistry of the structure was checked using PROCHECK (43), and the
647 Ramachandran plot and was validated using the PDB validation server. Coordinates of
648 EipB have been deposited in the PDB (PDB code 6NTR). Crystallographic data and

649 refined model statistics are presented in Table S2. Diffraction images have been uploaded
650 to the SBGrid data server (Data DOI: 10.15785/SBGRID/445).
651
652 **Alkaline phosphatase cell localization assay**
653 To determine the cellular localization of EipB, we used a *B. ovis* strain transformed with the
654 pSRK plasmid carrying *B. abortus eipB* C-terminally fused to *E. coli phoA*. Two versions of
655 this plasmid were made: one carrying the full-length *eipB*, which expressed the protein with
656 its signal peptide, and one carrying a short version of *eipB*, which expressed the protein
657 lacking the signal peptide. Alkaline phosphatase assays were performed as previously
658 described (8). Briefly, aliquots of overnight culture of *B. ovis* (in presence or absence of 1
659 mM IPTG) were mixed with 5-Bromo-4-chloro-3-indolyl phosphate (BCIP, final
660 concentration 200 μM). After 2 hours of incubation, the color change was visually
661 assessed and pictures were taken. Same experiment was performed with spent medium
662 supernatants.
663
664 **Size exclusion chromatography**
665 A DNA fragment corresponding to *B. abortus eipB* lacking the signal peptide (residues 30 -
666 280) was cloned into pET28a and transformed into the protein overexpression *E. coli*
667 Rosetta(DE3) *plysS* strain. Protein expression and purification was conducted using a Ni^{2+}
668 affinity purification protocol as previously published (8). The purified protein was then
669 dialyzed against a Tris-NaCl buffer (10 mM Tris pH 7.4, 150 mM NaCl). EipB oligomeric
670 state was analyzed by size exclusion chromatography as previously described. Briefly,
671 after concentration, a protein sample (500 μl at 5 mg/ml) was injected onto a GE
672 Healthcare Superdex 200 10/300 GL column (flow rate: 0.5 ml/min). Elution profile was

673 measured at 280 nm and 500 µl fractions of were collected during the run; the dialyzing
674 buffer as that described above was used for all runs. Protein standards (blue dextran /
675 aldolase / conalbumin / ovalbumin) were also injected into the column, and the
676 corresponding calibration curve was use for molecular size estimation of the purified EipB.
677

678 **Pull-down assay between EipB and TtpA**

679 To evaluate the interaction between *B. abortus* EipB and TtpA, the different proteins (His_6-
680 $EipB^{WT}$ or His_6-EipB cysteine mutants, and MBP-TtpA) were overexpressed and purified
681 using nickel affinity and amylose affinity gravity columns, respectively. Two milliliters of
682 amylose resin were saturated with 10 ml of a clarified cell lysate corresponding to a 500 ml
683 culture pellet of IPTG induced *Rosetta* pMalc2g-*ttpA*. Beads were thoroughly washed with
684 50 ml of a Tris-NaCl buffer (10 mM Tris pH7.4, 150 mM NaCl) and 200 µl of these beads
685 were mixed with 500 µl of nickel purified EipB at ~0.5 mg/ml (see reference (8) for a
686 detailed nickel-affinity purification protocol). After 30 min incubation in presence or
687 absence of 1 mM DTT, the flow-through was saved and the beads were thoroughly
688 washed with a Tris-NaCl buffer supplemented or not with 1 mM DTT. The protein was
689 eluted with 200 µl of same buffer containing 20 mM of maltose. The different protein
690 samples (elutions and flow-throughs) were run on a 12% SDS-PAGE and Coomassie
691 stained.
692

693 **Bacterial two-hybrid protein interaction assay**

694 To assay EipB interaction with TtpA, we also used a bacterial two-hybrid system as
695 previously published (8). Briefly, *B. abortus eipB* DNA fragments was cloned into pKT25
696 vector and *B. abortus ttpA* was cloned into pUT18 or pUT18C vectors. The different

697 pUT18, pUT18C and pKT25 combinations were then co-transformed into chemically
698 competent *E. coli* reporter strain BTH101 and spotted on LB agar plates (ampicillin 100
699 µg/ml + kanamycin 50 µg/ml) supplemented with X-Gal (40 µg/ml).
700
701 **Disulfide bond reduction assays**
702 DNA fragments corresponding to *B. abortus eipB* cysteine mutants (C69S, C278S, and
703 C69S+C278S) and lacking the signal peptide (residues M1-A30) were cloned into pET28a
704 and transformed into the protein overexpression *E. coli* Rosetta(DE3) *plysS* strain. Protein
705 expression and Ni^{2+} affinity purification were conducted using protocols previously
706 published (8). Briefly, for each protein, a pellet corresponding to a 250 ml culture was
707 resuspended in 1.5 ml of BugBuster Master Mix (MD Millipore) supplemented with 50 µl of
708 DNAse I (5mg/ml). After 20 min on ice, cell debris was pelleted and the supernatant was
709 mixed with 200 µl of Ni-NTA Superflow resin (Qiagen). Beads were washed with 8 ml of a
710 10 mM imidazole Tris-NaCl buffer (10 mM Tris pH7.4, 150 mM NaCl) and 5 ml of a 75 mM
711 imidazole Tris-NaCl buffer. Proteins were eluted with 200 µl of a 500 mM imidazole Tris-
712 NaCl buffer. 50 µl of each purified protein (at 0.5 mg/ml) were then mixed with 12.5 µl of a
713 4x protein loading dye containing or not 1 mM of DTT. Samples were boiled for 5 min and
714 10 µl were loaded on a 12% SDS-PAGE.
715
716 **Thermal shift protein stability assay**
717 The thermal shift assay to assess protein stability was performed on 20 µl samples
718 containing 25 µM of purified *B. abortus* $EipB^{WT}$ or $EipB^{C69S+C278S}$, 50x Sypro Orange
719 (Invitrogen) and 2 mM DTT when needed. Each protein sample and solution was prepared
720 with the same dialysis buffer (10 mM Tris (pH 7.4), 150 mM NaCl, 1 mM EDTA). Ninety-

721 six-well plates (MicroAmp EnduratePlate Optical 96-well fast clear reaction plates; Applied
722 Biosystems) were used and heated from 25 to 95°C with a ramp rate of 0.05°C/s and read
723 by a thermocycler (QuantumStudio 5 real-time PCR system; Applied Biosystems - Thermo
724 Fisher scientific) using excitation and emission wavelengths of 470 ± 15 nm and 558 ± 11
725 nm, respectively. Protein Thermal Shift software v1.3 (Applied Biosystems - Thermo Fisher
726 scientific) was used for calculation of the first derivative of the curve to determine the
727 melting temperature.
728
729 **Bioinformatics**
730 Figures of the structures, structural alignments, electrostatic potential representations and
731 r.m.s.d. calculations were performed using PyMOL (PyMOL Molecular Graphics System,
732 version 1.7.4; Schrödinger, LLC). Surface hydrophobicity was evaluated using the YRB
733 python script (44). The XtalPred server (45) and Dali server (46) were used to identify
734 proteins with the highest structural and sequence homology. The BLAST server
735 (https://blast.ncbi.nlm.nih.gov/Blast.cgi) was used to identify homologs of *B. abortus* EipB
736 in different taxa within the *Alphaproteobacteria*. The weblogo was generated by aligning
737 447 *Alphaproteobacteria* DUF1849 protein sequences retrieved from the EMBL-EBI
738 website (https://www.ebi.ac.uk/interpro/entry/IPR015000/proteins-matched). Alignment
739 was generated with Clustal Omega (https://www.ebi.ac.uk/Tools/msa/clustalo/). When
740 necessary, the C-terminus sequences were realigned by hand. The Clustal alignment file
741 was then converted to a fasta file using
742 http://sequenceconversion.bugaco.com/converter/biology/sequences/clustal_to_fasta.php.
743 This file was then submitted to skylign server (http://skylign.org/) to generate a weblogo.

744 The alignment was processed with the following options: remove mostly-empty columns /
745 alignment sequences are full length / score.
746

747 **Acknowledgments**

748 We thank the members of the Crosson laboratory for helpful discussions. The authors wish
749 to thank members of the SBC at Argonne National Laboratory for their help with data
750 collection at the 19-ID beamline. This work was supported by National Institutes of Health
751 Grants U19AI107792 and R01AI107159 to S.C.
752

753 **Author contributions**

754 JH, JWW and SC contributed to the design and conceptualization of the study; JH, JWW,
755 AF, DMC, JXC, EU, AB, LB, GB, YK and SC performed the experiments, acquired and
756 analyzed the data; JH, JWW, AF and SC interpreted the data; JH and SC wrote the
757 original draft of the manuscript.
758

759

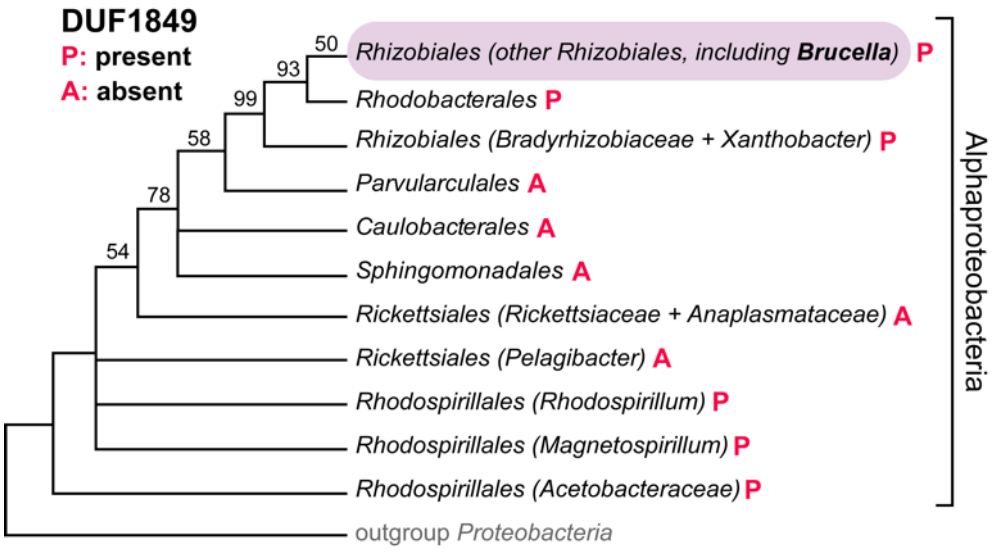

760

761 **Figure 1:** The DUF1849 sequence family is almost entirely restricted to
762 *Alphaproteobacteria*. Bayesian phylogenetic tree showing the distribution of DUF1849
763 genes in different orders within the class *Alphaproteobacteria* (P: present, A: absent).
764 Bayesian support values are shown when <100%; nodes were collapsed when support
765 was <50%; adapted from Williams and colleagues (47). In *Brucella abortus* (order
766 *Rhizobiales*), DUF1849 is encoded by gene locus *bab1_1186* (i.e. *eipB*).
767

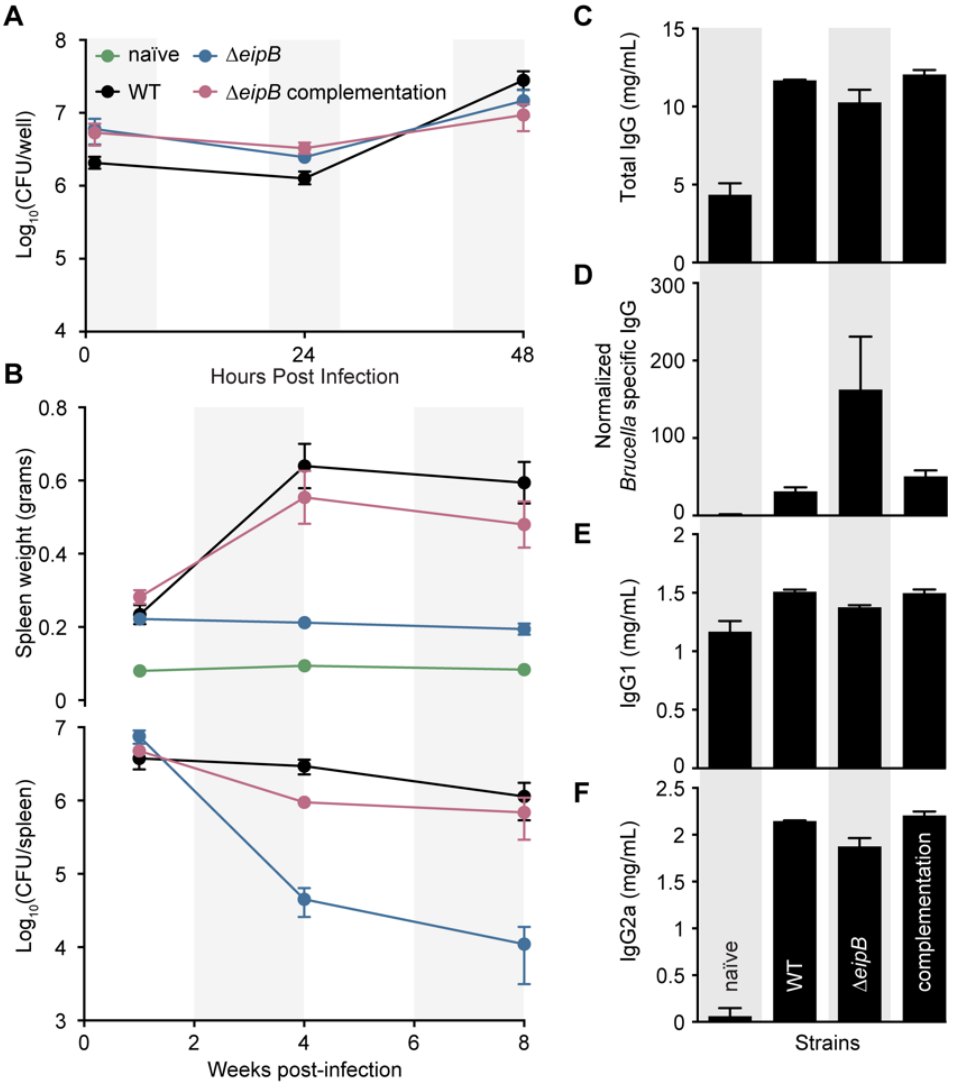

Figure 2: *eipB* is a genetic determinant of *B. abortus* virulence. A) *In vitro* macrophage infection assay: infection of THP-1 cells with wild-type *B. abortus* 2308 (black line), Δ*eipB* (blue line) and the *eipB* complementation strain (pink line). The number of *B. abortus* CFUs recovered from the THP-1 cells at 1, 24, and 48 hours post infection is plotted. Each data point (n= 3 per strain) is the mean ± the standard error of the mean. B) *In vivo* mouse infection assay: Female BALB/c mice were injected intraperitoneally with wild-type, Δ*eipB*, or Δ*eipB*-complementation strains. Spleen weights (upper graph) and bacterial burden (lower graph) were measured at 1, 4, and 8 weeks post-infection. Graphs represent data from uninfected, naïve mice (in green) or mice infected with wild-type (black), Δ*eipB* (blue), or complementation (pink) strains. Data presented are the mean ± the standard error of the mean; n= 5 mice per strain per time point. C-F) Antibody quantification in mouse serum harvested at 8 weeks post-infection from naïve control mice or mice infected with wild-type, Δ*eipB*, or complementation strains. Amounts of total IgG (C), *Brucella*-specific IgG (D), IgG1 (E), and IgG2a (F) were determined by ELISA. Each data point (naïve: n= 3, WT: n= 2, Δ*eipB* and complementation: n= 4) is the mean ± the standard error of the mean.

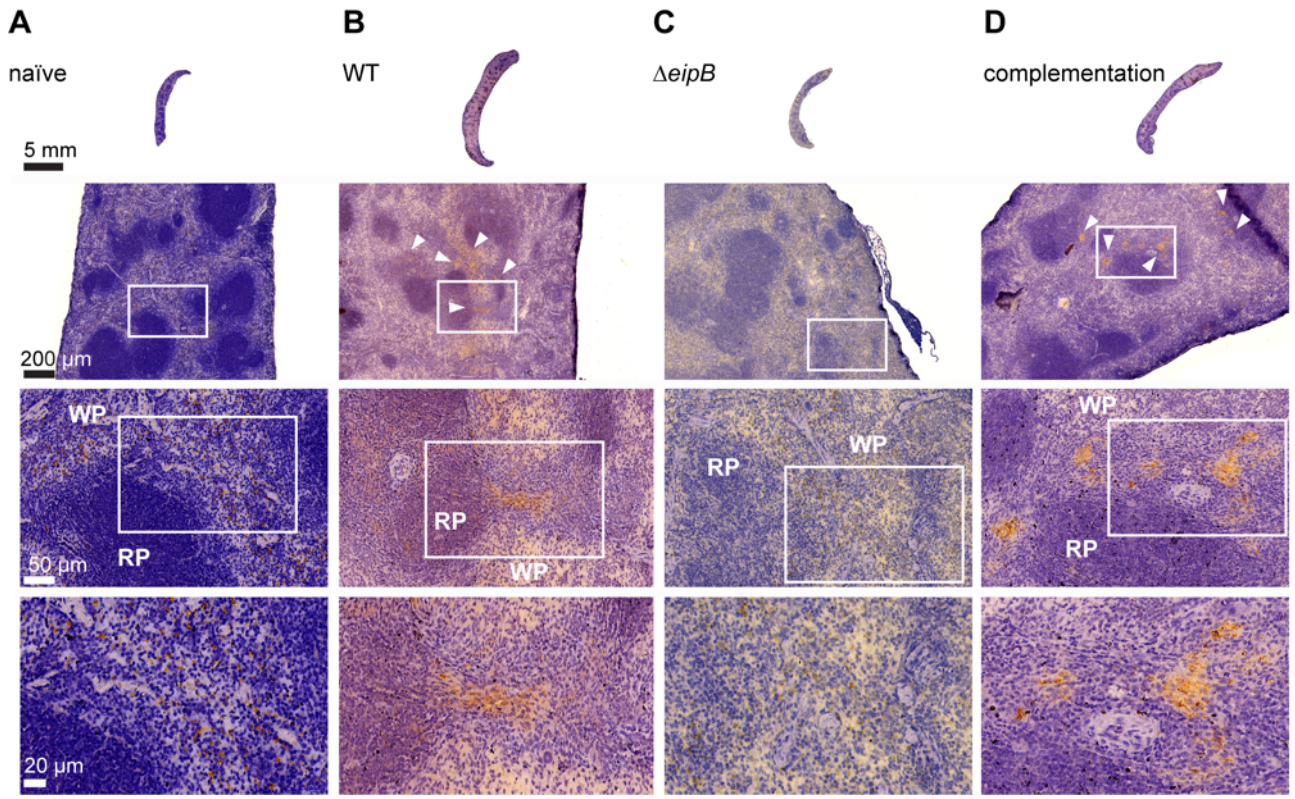

Figure 3: Histology of BALB/c mouse spleens at 8 weeks post-infection. Spleens (n= 1 per strain) were harvested, fixed, and stained with hematoxylin and eosin. Pictures of uninfected (A), wild-type (B), Δ*eipB* (C), or complementation (D) *B. abortus*-infected spleens were taken; white boxes represent specific regions enlarged in the images below. *Brucella* antigen was visualized by immunohistochemistry with an anti-*Brucella* antibody (brown regions, highlighted with white arrow heads). WP= white pulp, RP= red pulp.

794

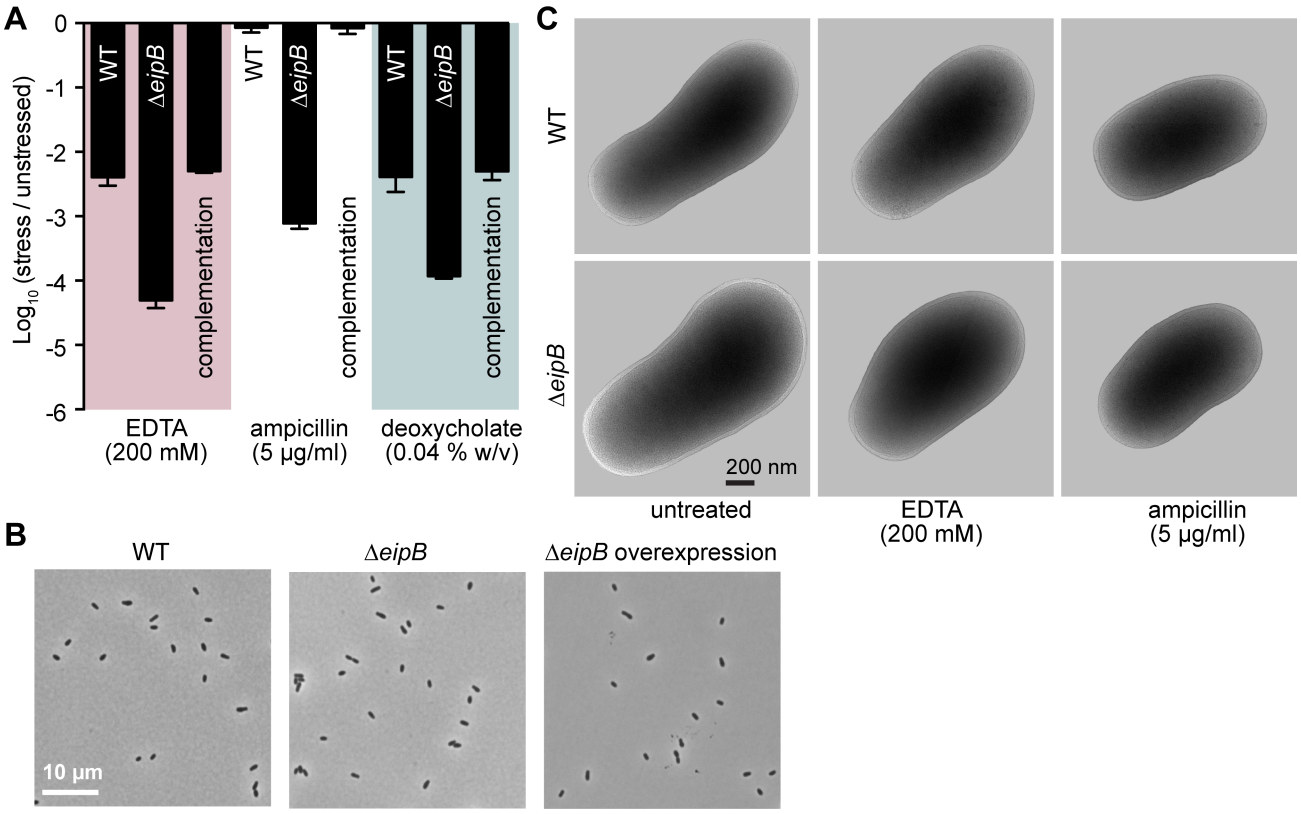

795

796 **Figure 4:** Assessing the effect of cell envelope stressors on *B. abortus* Δ*eipB* growth and
797 survival. A) Envelope stress survival assays. Serially diluted cultures of *B. abortus* wild-
798 type, Δ*eipB,* and complementation strains were spotted on plain TSA plates or TSA plates
799 containing EDTA (2 mM), deoxycholate (0.04% w/v), or ampicillin (5 µg/ml). After 3 to 5
800 days of growth at 37°C / 5% CO_2, CFUs for each condition were enumerated and plotted.
801 This experiment was repeated four times; each data point is the mean ± the standard error
802 of the mean. B) Light micrograph of *B. abortus* wild-type (left), Δ*eipB* (middle) and
803 overexpression (right; induced with 5 mM IPTG) liquid cultures grown overnight in Brucella
804 broth. C) CryoEM images of *B. abortus* wild-type and Δ*eipB* cells cultivated in liquid broth
805 that either remained untreated or were treated with 2 mM EDTA or 5 µg/ml ampicillin for 4
806 hours.
807

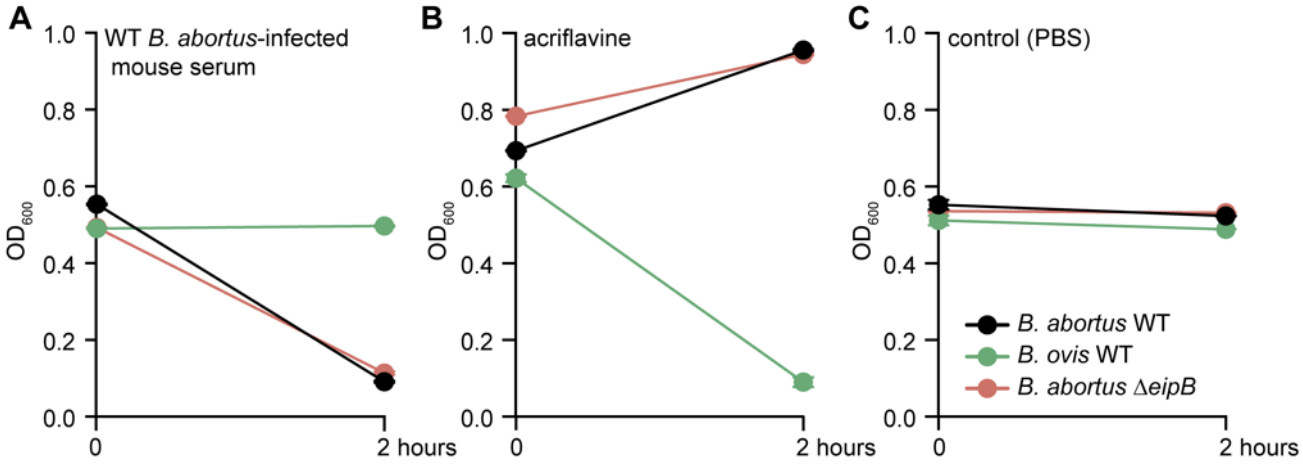

Figure 5: Deletion of *eipB* has no effect on the agglutination phenotype of *B. abortus*. The different *B. abortus* strains (wild-type in black, and Δ*eipB* in pink) and the wild-type *B. ovis* strain (in green) were incubated for 2 hours at room temperature in 1 ml of PBS supplemented with either (A) 20 µl of serum from a *B. abortus*-infected mouse, (B) 5 mM acriflavine (final concentration), or (C) no treatment. OD_{600} was measured at the beginning and the end of the experiment. The starting OD used was ~0.5. This experiment was performed in triplicate; each data point is the mean ± the standard error of the mean.

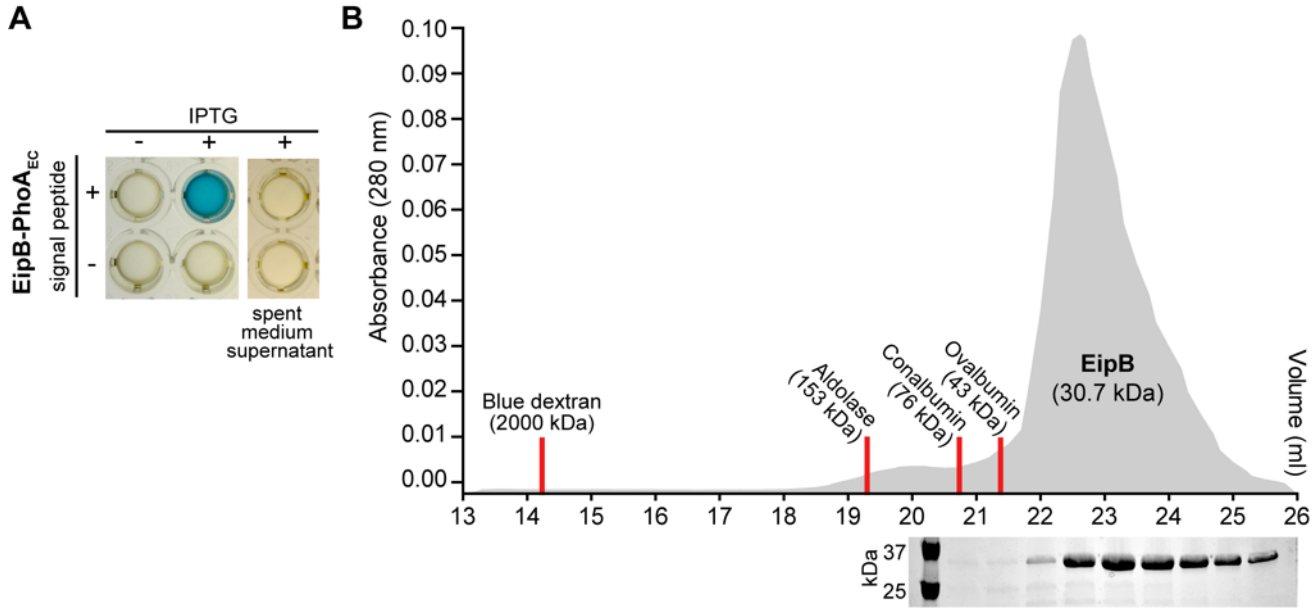

Figure 6: EipB is monomeric in solution and is secreted to the *Brucella* periplasm. A) Alkaline phosphatase assay. Overnight cultures of *B. ovis* expressing EipB with (+) or without (-) its signal peptide and fused to *E. coli* PhoA, were grown in presence (+) or absence (-) of 1 mM IPTG inducer. In a 96-well plate, these cultures were mixed with BCIP (200 µM final concentration) and developed for 2 hours at 37°C / 5% CO_2. Only the strain expressing EipB-PhoA$_{Ec}$ with a signal peptide turned blue, providing evidence that the protein is located in the periplasm. As a control, spent medium supernatants were mixed with BCIP to test whether EipB-PhoA$_{Ec}$ is secreted into the medium. After 2 hours incubation, no color change was observed, indicating that EipB-PhoA$_{Ec}$ is not exported outside the cell. These experiments were performed at least three times with independent clones. A representative image is shown. B) Size exclusion chromatography elution profile of purified EipB (in grey). Elution fractions were loaded on a SDS-PAGE, and a single band migrating at ~30 kDa was visible. Elution peaks of the molecular weight standards (blue dextran: 2000 kDa, aldolase: 157 kDa, conalbumin: 76 kDa, ovalbumin: 43 kDa) are shown as red line. This experiment was performed twice and yielded similar elution profiles.

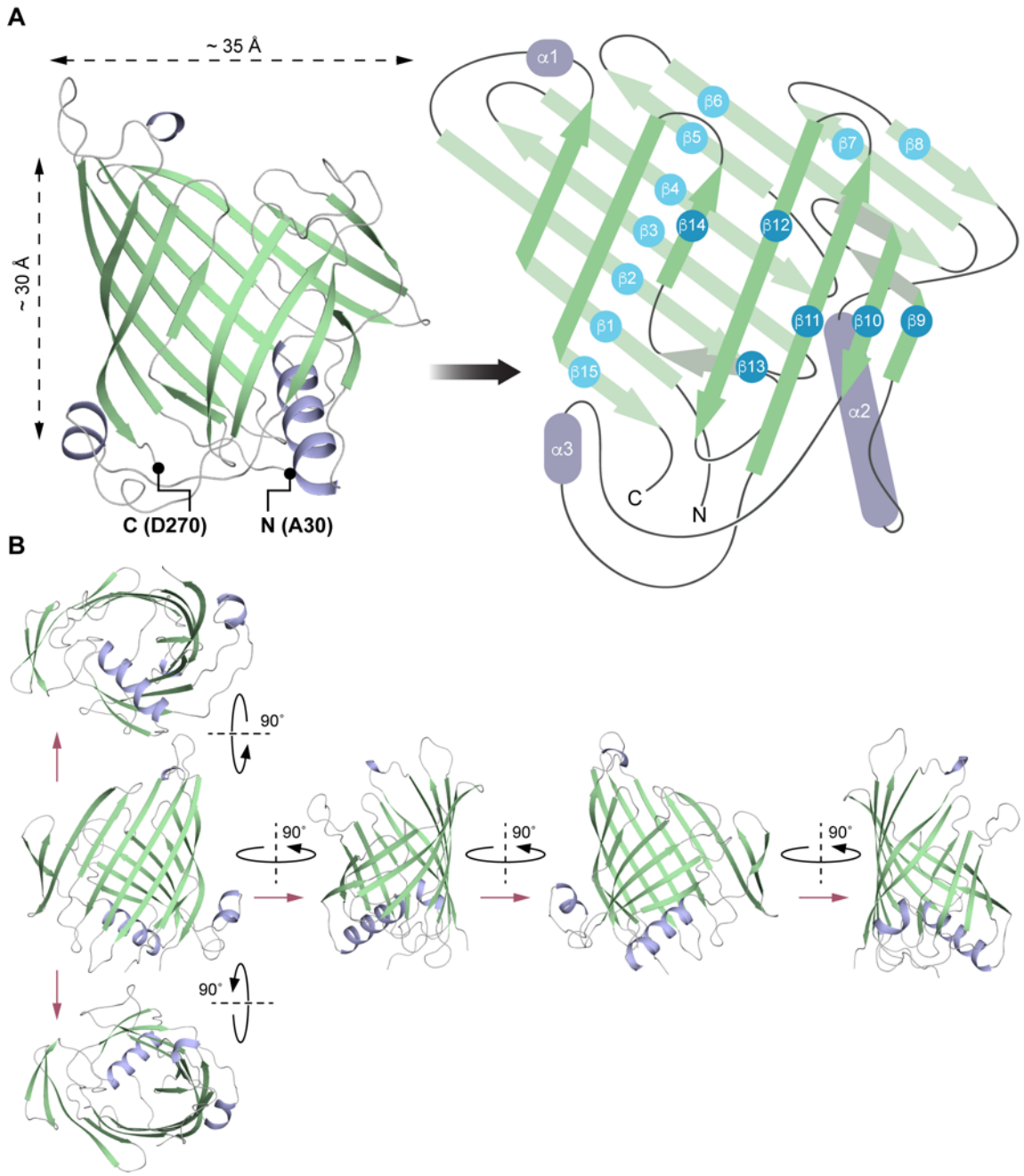

Figure 7: EipB adopts a β-spiral fold. A) Left: X-ray structure of EipB. EipB consist of 15 β-strands (in green) and 3 α-helices (in violet). The N-terminus (A30) and the C-terminus (D270) are reported on this structure. Right: simplified representation of EipB; color code is the same as before. B) Different orientations of EipB structure; color code is the same as before.

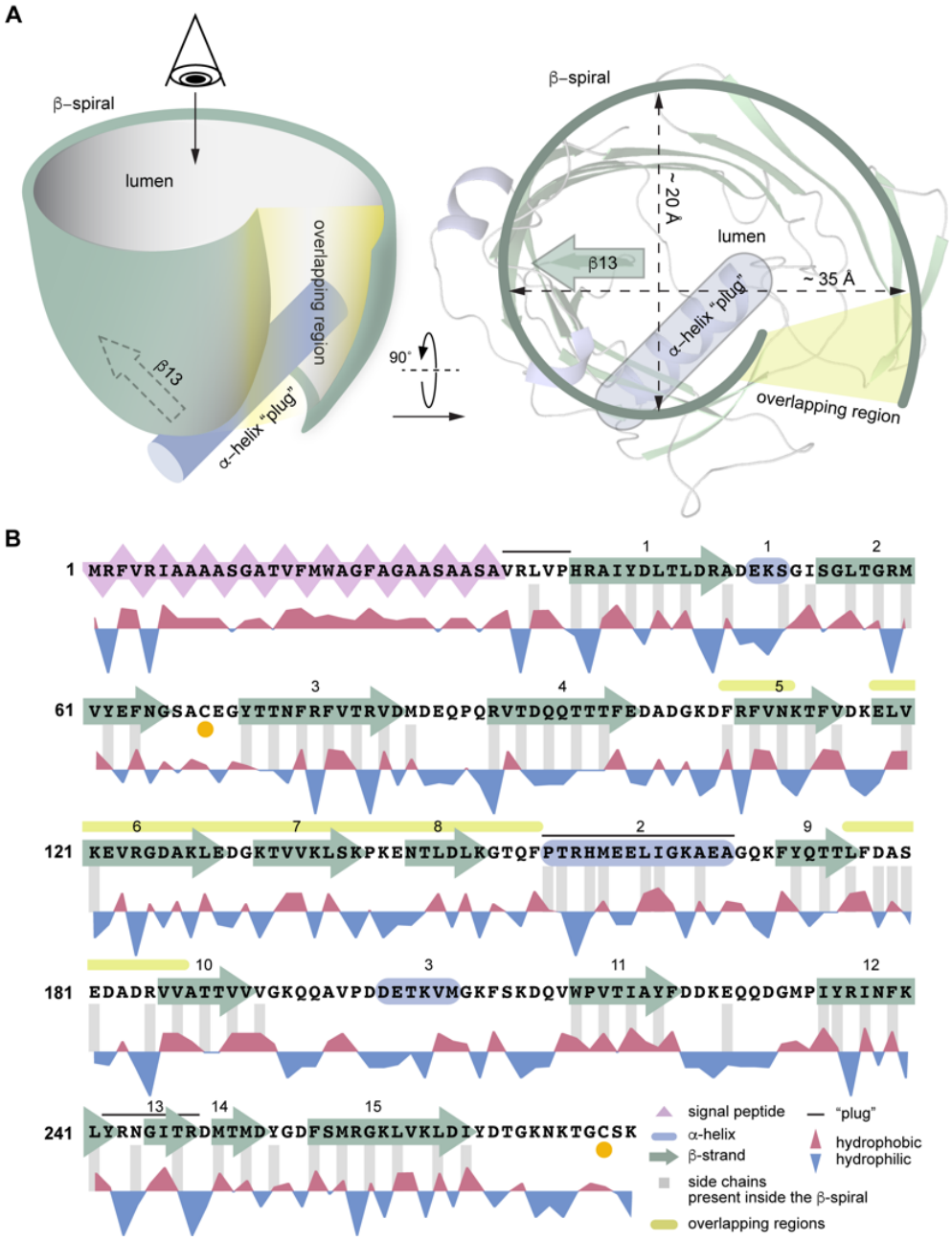

Figure 8: Simplified representation of EipB structure. A) EipB adopts a cup-like structure, fourteen β-strands (in green) form an overlapping β-spiral (β5-β6-β7-β8 overlap with β9-β10 connecting loop, highlighted in yellow in panel A and B). α2 (in violet) and β13 (in green) form the bottom of this "cup". B) Amino acid sequence of EipB. The sequence corresponding to the predicted signal peptide is highlighted in pink. β-strands and α-helices are represented by green arrows and violet cylinders, respectively. Hydrophobic (red) and hydrophilic (blue) residues are reported below the sequence. Residues with side chains present inside EipB cavity are highlighted with grey bars. Cysteines C69 and C278 are highlighted with orange dots.

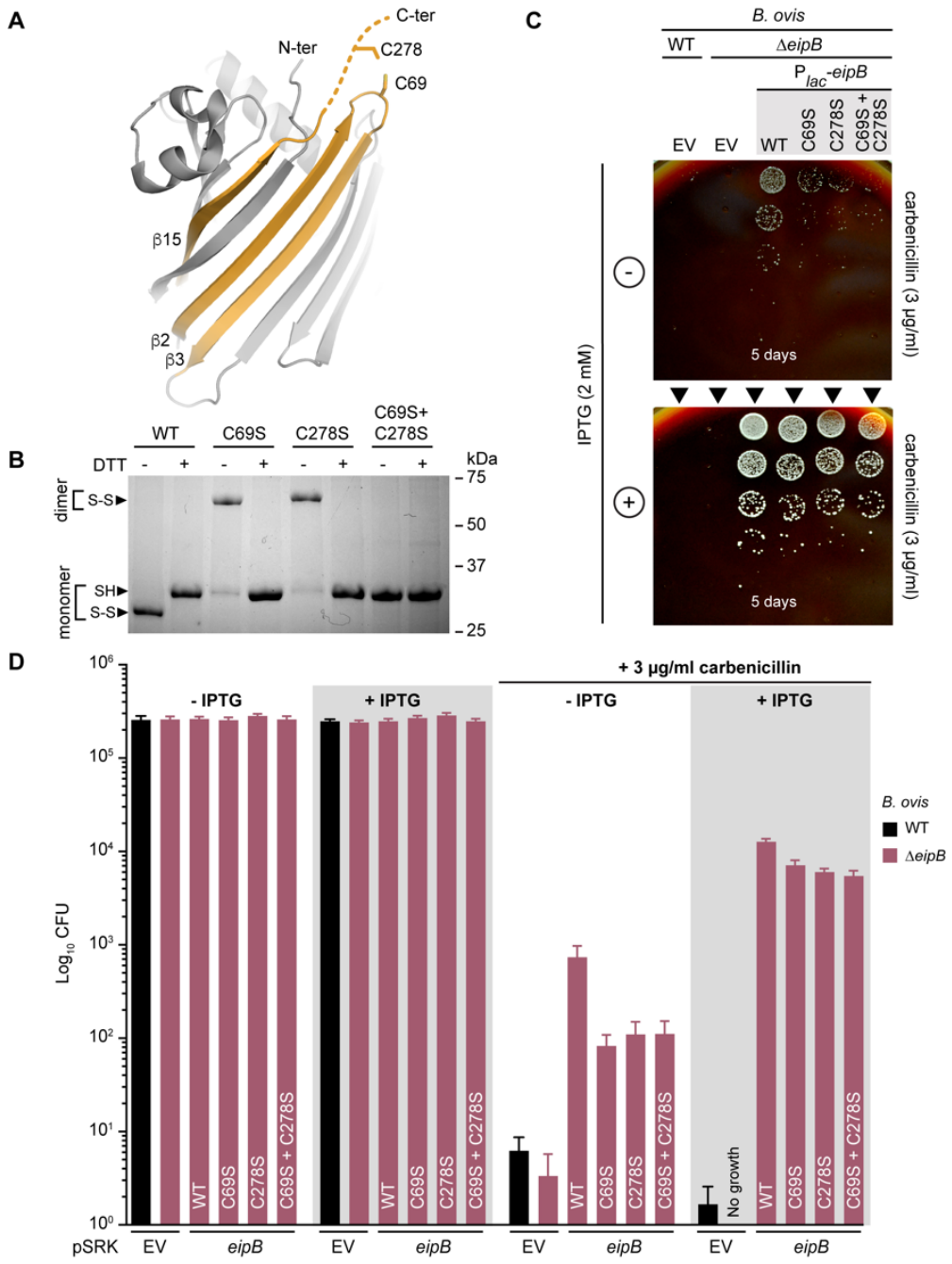

Figure 9: EipB has an internal disulfide bond. A) Cysteines C69 and C278 are spatially proximal in the EipB structure and form a disulfide bond. C278 is present at the EipB C-terminus that follows β15, and C69 is present in a loop connecting β2 and β3. B) His-tagged wild-type EipB and EipB cysteine mutant proteins (C69S, C278S, and C69S+C278S) were purified and mixed with a protein loading buffer plus or minus 1 mM DTT. Protein samples were resolved by 12% SDS-PAGE. This experiment was performed three times. Picture of a representative gel is presented. C) Growth on SBA plates containing 3 µg/ml of carbenicillin ± 2 mM IPTG of a serially diluted (10-fold dilution) *B. ovis* Δ*eipB* strain ectopically expressing wild-type EipB (P_{lac}-*eipB*), C69S mutant (P_{lac}-*eipB*^{C69S}), C278S mutant (P_{lac}-*eipB*^{C69S}), or C69S+C278S mutant (P_{lac}-*eipB*$^{C69S+C278S}$). *B.*

867 *ovis* wild-type (WT) and Δ*eipB* carrying the pSRK empty vector (EV) was used as a
868 control. Days of growth at 37°C / 5% CO_2 are reported for each plate. A representative
869 picture of the different plates is presented. D) Enumerated CFU after growth on SBA plates
870 containing 3 µg/ml of carbenicillin ± 2 mM IPTG of serially diluted (10-fold dilution) *B. ovis*
871 Δ*eipB* strains expressing different versions of *eipB* from a plasmid (wild-type and cysteine
872 mutants; see panel C legend). Empty vector (EV) strains and SBA plates with no
873 carbenicillin, plus or minus IPTG, were used as controls. This experiment was
874 independently performed twice with two different clones each time, and all plate assays
875 were done in triplicate. Each data point is the mean ± the standard error of the mean.
876

877

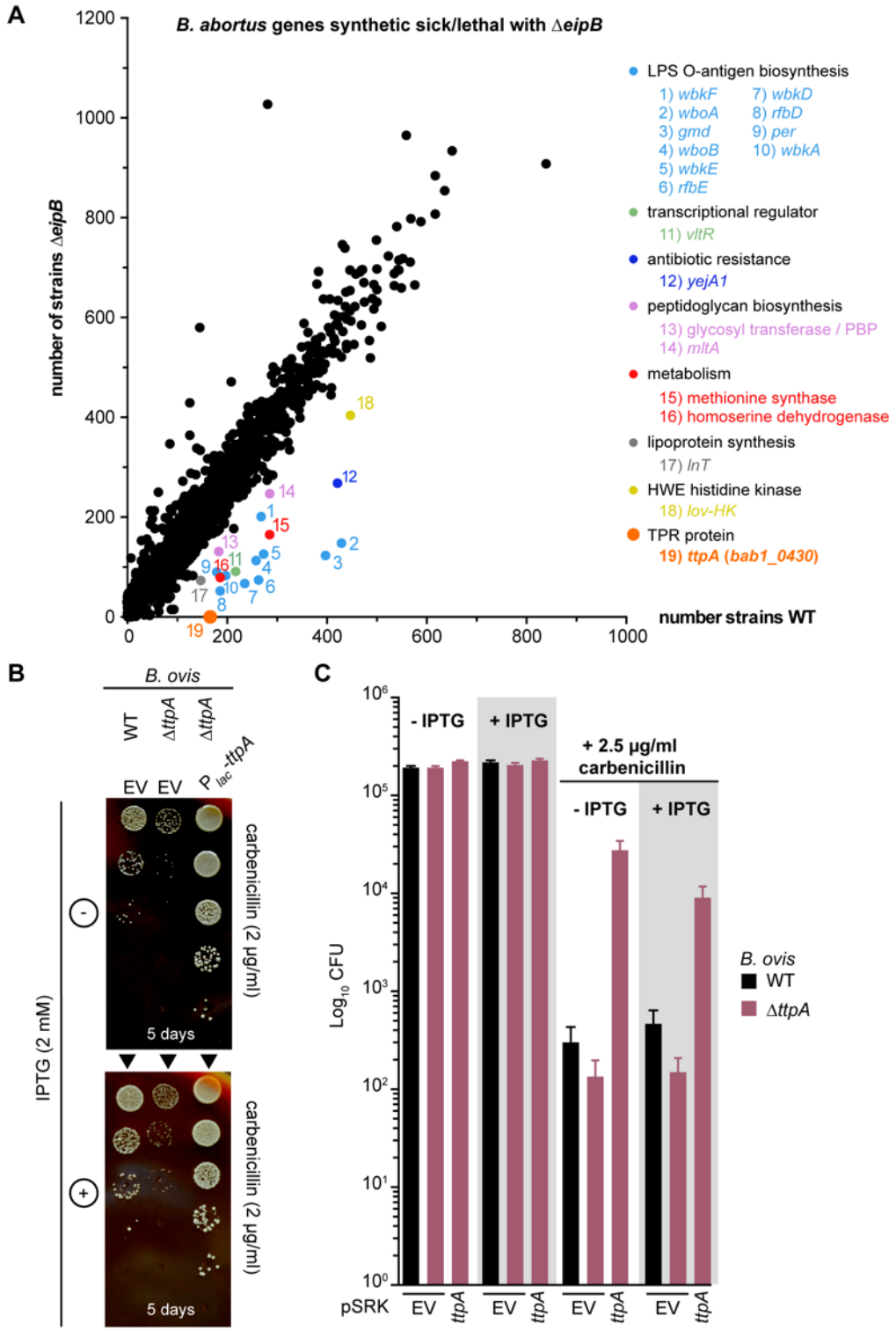

878

879 **Figure 10:** *B. abortus eipB* deletion is synthetically lethal with Tn-Himar disruption of
880 *bab1_0430*, which encodes a TPR protein. A) Identification of *B. abortus* genes that are

881 synthetically lethal or sick with *eipB* deletion. Tn-Himar insertion strains per gene (black
882 dots) obtained in a *B. abortus* Δ*eipB* background are plotted as a function of strains per
883 gene in a wild-type background. *bab1_0430*, for which we observed significantly fewer
884 insertions in Δ*eipB* than in wild-type, is represented as an orange dot. Other synthetic sick
885 genes are also evident in the plot, including genes involved in LPS O-antigen synthesis in
886 light-blue (*wbkF bab1_0535*; *wboA bab1_0999*; *gmd bab1_0545*; *wboB bab1_1000*; *wbkE*
887 *bab1_0563*; *rfbE bab1_0542*; *wbkD, bab1_0534*; *rfbD bab1_0543*; *per bab1_0544*; *wbkA*
888 *bab1_0553*), genes related to peptidoglycan synthesis in pink (*mltA bab1_2076*; penicillin-
889 binding protein *bab1_607*). Apolipoprotein N-acyltransferase *lnt* (*bab1_2158*) is in grey;
890 LysR transcriptional regulator *vtlR* (*bab1_1517*) is in light green; extracellular solute
891 binding protein *yejA1* (*bab1_0010*) is in dark blue; general stress response regulator *lovhK*
892 (*bab1_0652*) is in yellow; metabolic genes (methionine synthase *bab1_0188*, and
893 homoserine dehydrogenase *bab1_1293*) are in red. B) Growth on SBA plates containing 2
894 µg/ml of carbenicillin ± 2 mM IPTG of serially diluted (10-fold dilution) *B. ovis* Δ*ttpA* strains
895 carrying the pSRK empty vector (EV) or ectopically expressing wild-type TtpA (P_{lac}-*ttpA*).
896 The wild-type (WT) *B. ovis* pSRK empty vector (EV) strain was used as a control. Days of
897 growth at 37°C / 5% CO_2 are reported for each plate. A representative picture of the
898 different plates is presented. C) Enumerated CFU, after growth on SBA plates containing
899 2.5 µg/ml of carbenicillin ± 2 mM IPTG, of serially diluted (10-fold dilution) *B. ovis* wild-type
900 (black) and Δ*ttpA* (dark pink) strains. The Δ*ttpA* strain was either transformed with the
901 empty vector (EV) or with pSRK-*ttpA*. Empty vector (EV) wild-type strain and SBA plates
902 with no carbenicillin, and plus or minus IPTG were used as controls. This experiment was
903 independently performed twice with two different clones each time, and all plate assays
904 were done in triplicate. Each data point is the mean ± the standard error of the mean.
905

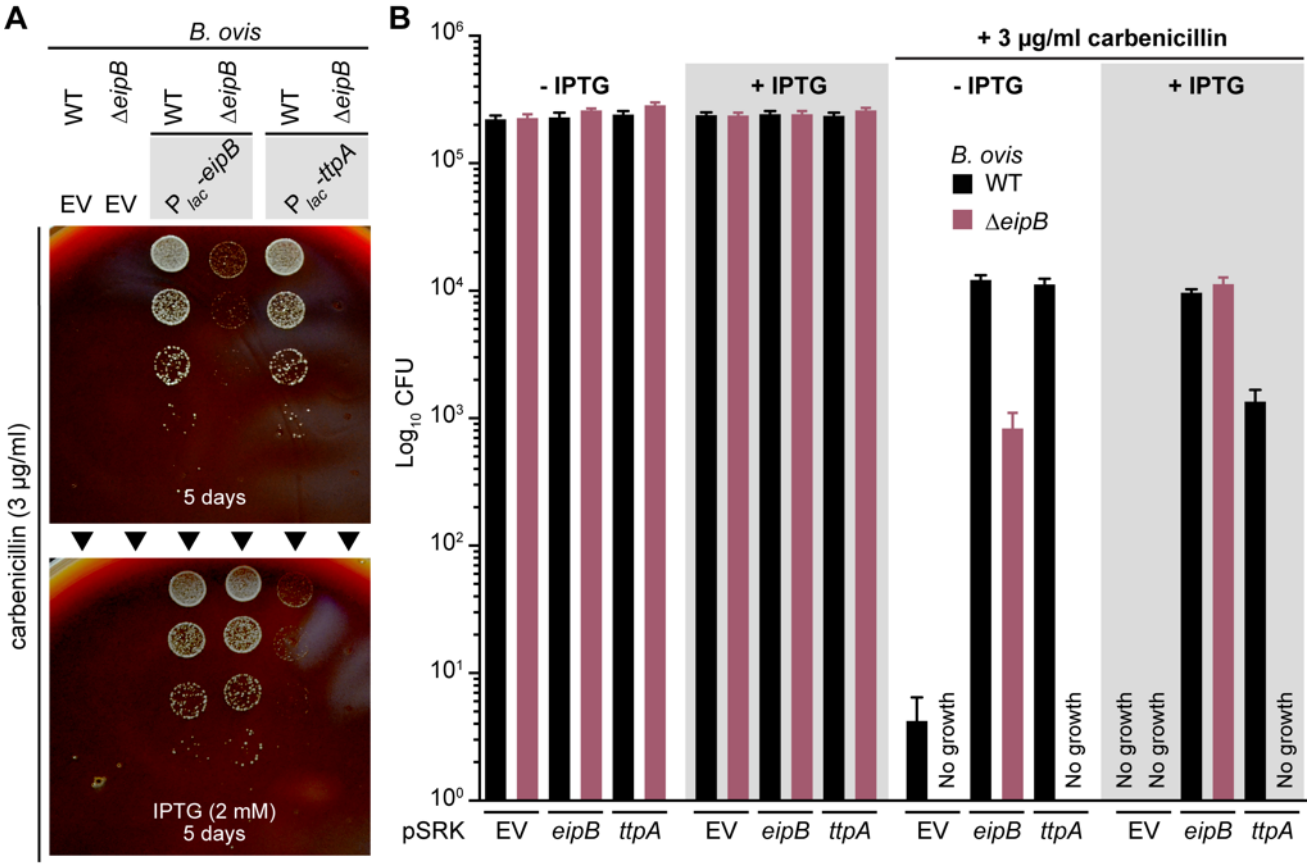

Figure 11: Overexpression of TtpA protects against carbenicillin treatment; protection requires EipB. A) Growth on SBA plates containing 3 µg/ml of carbenicillin ± 2 mM IPTG of serially diluted (10-fold dilution) *B. ovis* wild-type (WT) and Δ*eipB* strains expressing wild-type EipB (P_{lac}-*eipB*) or TtpA (P_{lac}-*ttpA*). *B. ovis* strains carrying the pSRK empty vector (EV) were used as a control. Days of growth at 37°C / 5% CO_2 are reported for each plate. A representative picture of the different plates is presented. B) Enumerated CFU after growth on SBA plates containing 3 µg/ml of carbenicillin ± 2 mM IPTG of serially diluted (10-fold dilution) *B. ovis* wild-type (black) and Δ*eipB* (dark pink) strains ectopically expressing *eipB* or *ttpA*. Empty vector (EV) strains and SBA plates with no carbenicillin, and plus or minus IPTG were used as controls. This experiment was independently performed twice with two different clones each time, and all plate assays were done in triplicate. Each data point is the mean ± the standard error of the mean.

920 **References**
921

922 1. Gorvel JP, Moreno E. 2002. *Brucella* intracellular life: from invasion to intracellular
923 replication. Vet Microbiol 90:281-97.
924 2. Pappas G, Papadimitriou P, Akritidis N, Christou L, Tsianos EV. 2006. The new
925 global map of human *brucellosis*. Lancet Infect Dis 6:91-9.
926 3. Batut J, Andersson SG, O'Callaghan D. 2004. The evolution of chronic infection
927 strategies in the alpha-proteobacteria. Nat Rev Microbiol 2:933-45.
928 4. Atluri VL, Xavier MN, de Jong MF, den Hartigh AB, Tsolis RM. 2011. Interactions of
929 the human pathogenic *Brucella* species with their hosts. Annu Rev Microbiol
930 65:523-41.
931 5. Roop RM, 2nd, Gaines JM, Anderson ES, Caswell CC, Martin DW. 2009. Survival
932 of the fittest: how Brucella strains adapt to their intracellular niche in the host. Med
933 Microbiol Immunol 198:221-38.
934 6. Byndloss MX, Tsolis RM. 2016. Brucella spp. Virulence Factors and Immunity. Annu
935 Rev Anim Biosci 4:111-27.
936 7. Lamontagne J, Butler H, Chaves-Olarte E, Hunter J, Schirm M, Paquet C, Tian M,
937 Kearney P, Hamaidi L, Chelsky D, Moriyon I, Moreno E, Paramithiotis E. 2007.
938 Extensive cell envelope modulation is associated with virulence in Brucella abortus.
939 J Proteome Res 6:1519-29.
940 8. Herrou J, Willett JW, Fiebig A, Varesio LM, Czyz DM, Cheng JX, Ultee E, Briegel A,
941 Bigelow L, Babnigg G, Kim Y, Crosson S. 2018. Periplasmic protein EipA
942 determines envelope stress resistance and virulence in *Brucella abortus*. Mol
943 Microbiol doi:10.1111/mmi.14178.
944 9. Finn RD, Coggill P, Eberhardt RY, Eddy SR, Mistry J, Mitchell AL, Potter SC, Punta
945 M, Qureshi M, Sangrador-Vegas A, Salazar GA, Tate J, Bateman A. 2016. The
946 Pfam protein families database: towards a more sustainable future. Nucleic Acids
947 Res 44:D279-85.
948 10. Price MN, Wetmore KM, Waters RJ, Callaghan M, Ray J, Liu H, Kuehl JV, Melnyk
949 RA, Lamson JS, Suh Y, Carlson HK, Esquivel Z, Sadeeshkumar H, Chakraborty R,
950 Zane GM, Rubin BE, Wall JD, Visel A, Bristow J, Blow MJ, Arkin AP, Deutschbauer
951 AM. 2018. Mutant phenotypes for thousands of bacterial genes of unknown
952 function. Nature 557:503-509.
953 11. Lestrate P, Dricot A, Delrue RM, Lambert C, Martinelli V, De Bolle X, Letesson JJ,
954 Tibor A. 2003. Attenuated signature-tagged mutagenesis mutants of *Brucella*
955 *melitensis* identified during the acute phase of infection in mice. Infect Immun
956 71:7053-60.
957 12. Neudorf KD, Vanderlinde EM, Tambalo DD, Yost CK. 2015. A previously
958 uncharacterized tetratricopeptide-repeat-containing protein is involved in cell
959 envelope function in *Rhizobium leguminosarum*. Microbiology 161:148-57.
960 13. Lapaque N, Moriyon I, Moreno E, Gorvel JP. 2005. *Brucella* lipopolysaccharide acts
961 as a virulence factor. Curr Opin Microbiol 8:60-6.
962 14. Papo N, Shai Y. 2005. A molecular mechanism for lipopolysaccharide protection of
963 Gram-negative bacteria from antimicrobial peptides. J Biol Chem 280:10378-87.
964 15. Palmer DA, Douglas JT. 1989. Analysis of *Brucella* lipopolysaccharide with specific
965 and cross-reacting monoclonal antibodies. J Clin Microbiol 27:2331-7.
966 16. Alton GG, Jones LM, Pietz DE. 1975. Laboratory techniques in brucellosis. Monogr
967 Ser World Health Organ:1-163.

968 17. Turse JE, Pei J, Ficht TA. 2011. Lipopolysaccharide-Deficient Brucella Variants
969 Arise Spontaneously during Infection. Front Microbiol 2:54.
970 18. Nielsen H. 2017. Predicting Secretory Proteins with SignalP. Methods Mol Biol
971 1611:59-73.
972 19. Marrichi M, Camacho L, Russell DG, DeLisa MP. 2008. Genetic toggling of alkaline
973 phosphatase folding reveals signal peptides for all major modes of transport across
974 the inner membrane of bacteria. J Biol Chem 283:35223-35.
975 20. Holm L, Laakso LM. 2016. Dali server update. Nucleic Acids Res 44:W351-5.
976 21. Bakolitsa C, Kumar A, McMullan D, Krishna SS, Miller MD, Carlton D, Najmanovich
977 R, Abdubek P, Astakhova T, Chiu HJ, Clayton T, Deller MC, Duan L, Elias Y,
978 Feuerhelm J, Grant JC, Grzechnik SK, Han GW, Jaroszewski L, Jin KK, Klock HE,
979 Knuth MW, Kozbial P, Marciano D, Morse AT, Nigoghossian E, Okach L,
980 Oommachen S, Paulsen J, Reyes R, Rife CL, Trout CV, van den Bedem H, Weekes
981 D, White A, Xu Q, Hodgson KO, Wooley J, Elsliger MA, Deacon AM, Godzik A,
982 Lesley SA, Wilson IA. 2010. The structure of the first representative of Pfam family
983 PF06475 reveals a new fold with possible involvement in glycolipid metabolism.
984 Acta Crystallogr Sect F Struct Biol Cryst Commun 66:1211-7.
985 22. Marchesini MI, Connolly J, Delpino MV, Baldi PC, Mujer CV, DelVecchio VG,
986 Comerci DJ. 2011. *Brucella abortus* choloylglycine hydrolase affects cell envelope
987 composition and host cell internalization. PLoS One 6:e28480.
988 23. Connolly JP, Comerci D, Alefantis TG, Walz A, Quan M, Chafin R, Grewal P, Mujer
989 CV, Ugalde RA, DelVecchio VG. 2006. Proteomic analysis of Brucella abortus cell
990 envelope and identification of immunogenic candidate proteins for vaccine
991 development. Proteomics 6:3767-80.
992 24. Sternon JF, Godessart P, Goncalves de Freitas R, Van der Henst M, Poncin K,
993 Francis N, Willemart K, Christen M, Christen B, Letesson JJ, De Bolle X. 2018.
994 Transposon Sequencing of Brucella abortus Uncovers Essential Genes for Growth
995 In Vitro and Inside Macrophages. Infect Immun 86.
996 25. Wang Z, Bie P, Cheng J, Lu L, Cui B, Wu Q. 2016. The ABC transporter YejABEF is
997 required for resistance to antimicrobial peptides and the virulence of *Brucella*
998 *melitensis*. Sci Rep 6:31876.
999 26. Goolab S, Roth RL, van Heerden H, Crampton MC. 2015. Analyzing the molecular
1000 mechanism of lipoprotein localization in *Brucella*. Front Microbiol 6:1189.
1001 27. Sheehan LM, Budnick JA, Blanchard C, Dunman PM, Caswell CC. 2015. A LysR-
1002 family transcriptional regulator required for virulence in *Brucella abortus* is highly
1003 conserved among the alpha-proteobacteria. Mol Microbiol 98:318-28.
1004 28. Kim HS, Willett JW, Jain-Gupta N, Fiebig A, Crosson S. 2014. The Brucella abortus
1005 virulence regulator, LovhK, is a sensor kinase in the general stress response
1006 signalling pathway. Mol Microbiol 94:913-25.
1007 29. Silhavy TJ, Kahne D, Walker S. 2010. The bacterial cell envelope. Cold Spring Harb
1008 Perspect Biol 2:a000414.
1009 30. Okuda S, Tokuda H. 2011. Lipoprotein sorting in bacteria. Annu Rev Microbiol
1010 65:239-59.
1011 31. LoVullo ED, Wright LF, Isabella V, Huntley JF, Pavelka MS, Jr. 2015. Revisiting the
1012 Gram-negative lipoprotein paradigm. J Bacteriol 197:1705-15.
1013 32. Zeytuni N, Zarivach R. 2012. Structural and functional discussion of the tetra-trico-
1014 peptide repeat, a protein interaction module. Structure 20:397-405.

1015 33. Cerveny L, Straskova A, Dankova V, Hartlova A, Ceckova M, Staud F, Stulik J.
1016 2013. Tetratricopeptide repeat motifs in the world of bacterial pathogens: role in
1017 virulence mechanisms. Infect Immun 81:629-35.
1018 34. Vanderlinde EM, Magnus SA, Tambalo DD, Koval SF, Yost CK. 2011. Mutation of a
1019 broadly conserved operon (RL3499-RL3502) from *Rhizobium leguminosarum*
1020 biovar viciae causes defects in cell morphology and envelope integrity. J Bacteriol
1021 193:2684-94.
1022 35. Jean NL, Bougault CM, Lodge A, Derouaux A, Callens G, Egan AJ, Ayala I, Lewis
1023 RJ, Vollmer W, Simorre JP. 2014. Elongated structure of the outer-membrane
1024 activator of peptidoglycan synthesis LpoA: implications for PBP1A stimulation.
1025 Structure 22:1047-54.
1026 36. Khan SR, Gaines J, Roop RM, 2nd, Farrand SK. 2008. Broad-host-range
1027 expression vectors with tightly regulated promoters and their use to examine the
1028 influence of TraR and TraM expression on Ti plasmid quorum sensing. Appl Environ
1029 Microbiol 74:5053-62.
1030 37. Wetmore KM, Price MN, Waters RJ, Lamson JS, He J, Hoover CA, Blow MJ,
1031 Bristow J, Butland G, Arkin AP, Deutschbauer A. 2015. Rapid quantification of
1032 mutant fitness in diverse bacteria by sequencing randomly bar-coded transposons.
1033 MBio 6:e00306-15.
1034 38. Willett JW, Herrou J, Briegel A, Rotskoff G, Crosson S. 2015. Structural asymmetry
1035 in a conserved signaling system that regulates division, replication, and virulence of
1036 an intracellular pathogen. Proc Natl Acad Sci U S A 112:E3709-18.
1037 39. Minor W, Cymborowski M, Otwinowski Z, Chruszcz M. 2006. HKL-3000: the
1038 integration of data reduction and structure solution--from diffraction images to an
1039 initial model in minutes. Acta Crystallogr D Biol Crystallogr 62:859-66.
1040 40. Emsley P, Cowtan K. 2004. Coot: model-building tools for molecular graphics. Acta
1041 Crystallogr D Biol Crystallogr 60:2126-32.
1042 41. Adams PD, Grosse-Kunstleve RW, Hung LW, Ioerger TR, McCoy AJ, Moriarty NW,
1043 Read RJ, Sacchettini JC, Sauter NK, Terwilliger TC. 2002. PHENIX: building new
1044 software for automated crystallographic structure determination. Acta Crystallogr D
1045 Biol Crystallogr 58:1948-54.
1046 42. Murshudov GN, Vagin AA, Dodson EJ. 1997. Refinement of macromolecular
1047 structures by the maximum-likelihood method. Acta Crystallogr D Biol Crystallogr
1048 53:240-55.
1049 43. Laskowski RA, Macarthur MW, Moss DS, Thornton JM. 1993. Procheck - a
1050 Program to Check the Stereochemical Quality of Protein Structures. Journal of
1051 Applied Crystallography 26:283-291.
1052 44. Hagemans D, van Belzen IA, Moran Luengo T, Rudiger SG. 2015. A script to
1053 highlight hydrophobicity and charge on protein surfaces. Front Mol Biosci 2:56.
1054 45. Slabinski L, Jaroszewski L, Rychlewski L, Wilson IA, Lesley SA, Godzik A. 2007.
1055 XtalPred: a web server for prediction of protein crystallizability. Bioinformatics
1056 23:3403-5.
1057 46. Holm L, Rosenstrom P. 2010. Dali server: conservation mapping in 3D. Nucleic
1058 Acids Res 38:W545-9.
1059 47. Williams KP, Sobral BW, Dickerman AW. 2007. A robust species tree for the
1060 *alphaproteobacteria*. J Bacteriol 189:4578-86.
1061